Scanning Microscopy

Volume 1990
Number 4 *Fundamental Electron and Ion Beam Interactions with Solids for Microscopy, Microanalysis, and Microlithography*

Article 6

1990

Secondary Electron Emission from Solids. I. Secondary Electron Spectroscopy

Michel Cailler
Université de Nantes, France

Jean-Pierre Ganachaud
Université de Nantes, France

Follow this and additional works at: https://digitalcommons.usu.edu/microscopy

 Part of the Biology Commons

Recommended Citation

Cailler, Michel and Ganachaud, Jean-Pierre (1990) "Secondary Electron Emission from Solids. I. Secondary Electron Spectroscopy," *Scanning Microscopy*: Vol. 1990 : No. 4 , Article 6.
Available at: https://digitalcommons.usu.edu/microscopy/vol1990/iss4/6

This Article is brought to you for free and open access by the Western Dairy Center at DigitalCommons@USU. It has been accepted for inclusion in Scanning Microscopy by an authorized administrator of DigitalCommons@USU. For more information, please contact digitalcommons@usu.edu.

Scanning Microscopy Supplement 4, 1990 (Pages 57-79)
Scanning Microscopy International, Chicago (AMF O'Hare), IL 60666 USA

0892-953X/90$3.00+.00

SECONDARY ELECTRON EMISSION FROM SOLIDS. I. SECONDARY ELECTRON SPECTROSCOPY.

Michel Cailler[1]* and Jean-Pierre Ganachaud[2]

[1] ISITEM de l'Université de Nantes, Laboratoire de Sciences des Surfaces et Interfaces en Mécanique, 44087 Nantes Cédex 03, France.
[2] Faculté des Sciences et Techniques de l'Université de Nantes, Laboratoire de Physique du Solide Théorique, 2 Rue de la Houssinière, 44072 Nantes Cedex, France

Abstract

The secondary electron emission spectroscopy can provide useful information about the transitions in the electronic structure from solids and deals with the detection of fine structures superimposed on the true secondary peak, in the kinetic energy range of the true secondary electrons.

Several mechanisms have been proposed for the creation of these fine structures: diffraction phenomena, plasmon decay, interband transitions to unoccupied levels, Auger transitions and more recently, autoionization emission. Some features could not be explained as being due to any bulk effect and were considered as indicative of a need to include surface wave-matching arguments in the analysis of secondary electron emission spectra.

The authors give a review of the recent literature on the topic, including their own experience on the subject.

Key Words: Electron-induced secondary electron emission, angle-energy distributions, energy distributions, angular distributions, secondary electron emission spectroscopy, diffraction phenomena, plasmon decay, interband transitions, Auger transitions, autoionization emission, secondary electron emission crystal current method.

* Address for correspondance:
Michel Cailler
ISITEM de l'Université de Nantes
Laboratoire de Sciences des Surfaces et
Interfaces en Mécanique
La Chantrerie CP 3023, 44087
Nantes Cédex 03
France
Phone No 40291616

Introduction

The secondary electron emission is the emission of electrons from a solid as a result of the bombardment by a primary electron beam. Many important applications of this phenomenon can be found as for instance, scanning electron microscopy, Auger spectroscopy, particle multipliers. The secondary electron emission was discovered by Austin and Stark in 1902 and remained for a long time a rather confidential topic. Some papers by Farnsworth and by Copeland were published between 1920 and 1940 (see for instance, Farnsworth (1925, 1926, 1928) and Copeland (1933 a, b, 1935, 1940)). Bruining (1954) wrote a book on the physics and application of secondary electron emission. Harrower (1956) studied the Auger and secondary electron emissions as well as the energy loss spectra from Mo and W and gave evidence for fine structures in each case. In the years 60-75, Bronshtein and co-authors published many papers; the list is too long to be quoted here but we can mention for instance Bronshtein and Segal (1960 a,b), Bronshtein and Fraiman (1961) Bronshtein and Denisov (1965). Theories of secondary electron emission from metals were developed by Baroody (1950), Wolff (1954), Stolz (1959), Streitwolf (1959), Puff (1964), Cailler (1969), Ganachaud (1977), Chung and Everhart (1977) and Schou (1980). Hachenberg and Brauer (1959) published a complete monography on the topic, including their own theoretical contribution. Sickafus (1977a,b) studied the linearization of the secondary electron emission from surfaces of metals. Very recently, many excellent review papers on the secondary electron emission were published, in which a great number of works have been quoted. For instance, Schou (1988) wrote a very interesting paper establishing very clearly the similarities but also the differences between proton and electron induced emission.

Seiler (1983, 1984) has presented experimental results on secondary electron emission related to scanning electron microscopy. Bindi et al. (1980, 1987) and Lanteri *et al.* (1988) have described in details the main theoretical models based on the Boltzmann transport equation. Devooght *et al.* (1987) and Dubus *et al.* (1987) presented their original work on the age-diffusion model for low-energy electron transport in solids.

Taking into account this abundant recent literature on the secondary electron emission, we have decided to limit our presentation to two features of the topic.

The secondary electron emission spectroscopy deals with the detection of fine-structures superimposed on the true secondary peak, in the kinetic energy range of the true secondary electrons and can provide useful information about the transitions in the electronic structure from solids. Several mechanisms have been proposed for the creation of these fine structures : diffraction phenomena, plasmon decay, interband transitions to unoccupied levels, Auger transitions and more recently, autoionization emission. Some features could not be explained as being due to any bulk effect and were considered as indicative of a need to include surface wave-matching arguments in the analysis of secondary electron emission spectra. In the present paper, we give a review of the work devoted to the secondary electron emission spectroscopy, including our own experience on the subject

In a second paper (these proceedings) we will consider the description of secondary electron emission by simulation models on computers.

Basic formulas of SEE

The basic quantity for the description of the secondary electron emission is the number of electrons emitted with energy E_S in the direction Ω_S, per unit time and per unit area of the surface. Using Rösler and Brauer's terminology (1981a,b, 1988) and neglecting spin, this is the energy and angle dependent current density $j(E_S,\Omega_S)$. This differential current density $j(E_S,\Omega_S)$ is normalized to unit of primary electron current impinging on the surface. In such a definition, the primary electrons are supposed to have an equal energy E_p and a given incidence angle θ_p. Unfortunately, there are only a few number of experimental results on $j(E_S,\Omega_S)$ and usually the experimental results are presented under one of the following forms :

-the energy distribution :

$$j(E_S) = \int j(E_S, \Omega_S)\, d\Omega_S \qquad (1)$$

-the angular distribution :

$$j(\Omega_S) = \int j(E_S, \Omega_S)\, dE_S \qquad (2)$$

-the electron yield :

$$\sigma(E_p) = \int_0^{E_P} j(E_S)\, dE_S = \delta(E_p) + \eta(E_p) \qquad (3)$$

where δ is the integral of $j(E_S)$ up to the conventional upper limit of 50 eV and η the integral from 50 eV to Ep. Typical plots of these different quantities are given in Fig.1.

For a long time it was considered that the angular distribution followed a cosine distribution, that the energy distribution was a smooth curve characterized by the position of its maximum and the value of its half-height width and that the yields could be described by universal laws. We wanted to show that the reality is likely more complicated than this general view.

1) Energy distributions and secondary electron emission spectroscopy (SES)

The secondary electron emission spectroscopy can provide useful information about the transitions in the electronic structure from solids. Quite usually, it is used in relation with the electron energy loss spectroscopy (EELS) and the ultraviolet photoelectron spectroscopy (UPS) and deals with the detection of fine-structures superimposed on the true secondary peak, in the kinetic energy range of the true secondary electrons.

Several mechanisms have been proposed for the creation of these fine structures. We can quote :

- diffraction phenomena
- plasmon decay
- interband transitions to unoccupied levels
- Auger transitions and more recently,
- autoionization emission.

In the present section, we shall illustrate the interesting aspects of SES with the help of some examples.

Diffraction phenomena

This interpretation was given by Goto and Ishikawa (1972) to explain the fine structures they observed in the secondary energy distribution from a Si [111] single crystal. Diffraction effects

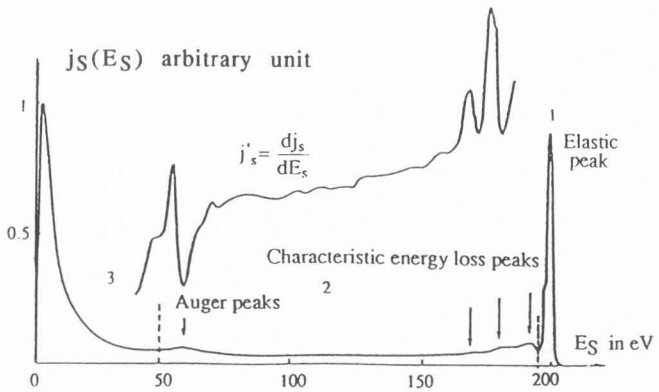

Fig.1a : Typical energy distribution of the electrons emitted from a solid target submitted to a bombardment by primary electrons. In the present case, the target was in copper ((111) single crystal) and the primary energy was of 200 eV. (From Roptin (1975)).

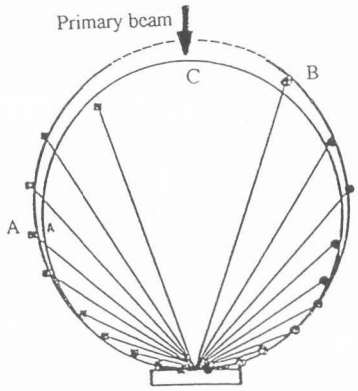

Fig.1b : Typical angular distributions of : (A) the secondary ( ) and (B) the inelastically backscattered primary electrons (o). (C) cosine law. In the present case, the target was in gold and the primary energy was of 200 eV. (From Cailler et al. (1977)).

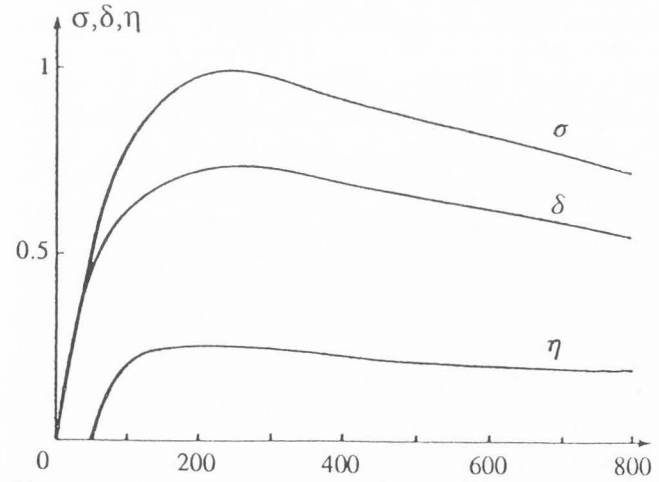

Fig.1c : Typical curves for the primary energy dependence of the yields. (From Cailler et al. (1977)).

were also utilized by Koshikawa *et al.* (1973) to explain the structures in the $\sigma(E_p)$ and $\eta(E_p)$ curves obtained from a Fe (110) single crystal. But, the same authors concluded from studies on secondary electron energy spectra from Fe(110) (Koshikawa *et al.* (1974)) that all spectra measured at various emission angles with a fixed angle of incidence were in agreement with each other when they were normalized to constant peak value. As a consequence, the escape process of secondary electrons were considered as being the same as that in a polycrystalline material. Feder and Pendry (1978), showed that in tungsten, the fine-structure in angle-resolved secondary electron spectra is related to the total reflectivity in low-energy electron diffraction.

Plasmon decay

A plasmon is a quantified collective oscillation arising in rather free electron gases. It was described in details by Pines and Nozieres (see for instance Pines (1953, 1956, 1960), Nozieres and Pines (1958, 1959)), Raether (1965) and Ritchie and co-authors (see Ritchie (1957), Ritchie and Eldridge (1962) and for the surface plasmon: Ritchie (1963, 1968, 1972, 1973), Ritchie and Marusak (1966) and Braundmeier *et al.* (1972), Ritchie *et al.* (1990) (these proceedings)).

Generally speaking, two mechanisms are essentially the origin of bulk plasmon loss process : the intrinsic loss, occurs simultaneously with the creation of a hole in core electronic levels, the extrinsic loss, instead, is connected with the energy loss due to inelastic scattering events which take place on the electron way towards the surface. The two mechanisms give rise to loss structures that coincide in the spectra but can be distinguished by investigating on the variation in the normalized intensity of the first bulk loss structure as a function of the primary electron energy (see Chiarello *et al.* (1984)).

The most often quoted example for plasmon decay is that of aluminium. Whereas the possibility of an important contribution of plasmon decay to the secondary electron emission was theoretically predicted by Cailler (1969) (see Fig.2), the earlier experimental results were obtained in the mid 70's by Henrich (1973), Cailler and coauthors (Roptin (1975), Pillon *et al.* (1976,1977)), Cailler *et al.* (1977), and Everhart *et al.* (1976).

Our measurements were performed by using a four-grid hemispherical retarding-field energy analyzer. Because of the very high sensitivity of the true secondary peak from Al, to the state of the surface, it was necessary to perform a deep cleaning of the sample by a series of argon ion sputtering and annealing cycles. After the first

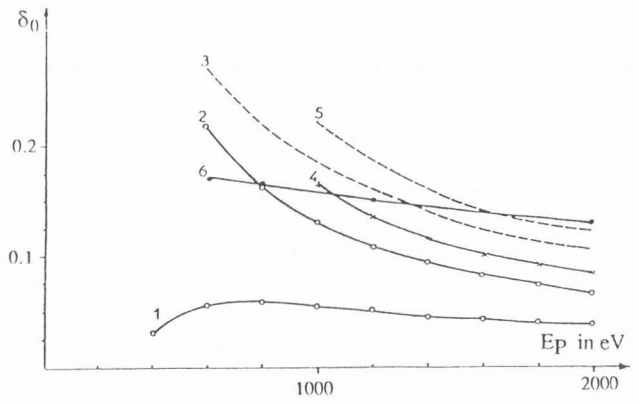

Fig.2 : Aluminium : Theoretical and experimental results on the primary energy dependence of the contribution δ_0 of the secondary electrons emitted from an aluminium target by penetrating primary electrons (From Cailler (1969)). (1) theoretical contribution from the individual excitations, (2) theoretical contribution from plasmon decay by creation of one electron-hole pair, (3) theoretical contribution from plasmon decay by creation of one or two electron-hole pairs, (4) sum of curves 1 and 2, (5) sum of curves 1 and 3, (6) experimental results by Bronstein and Fraiman (1961).

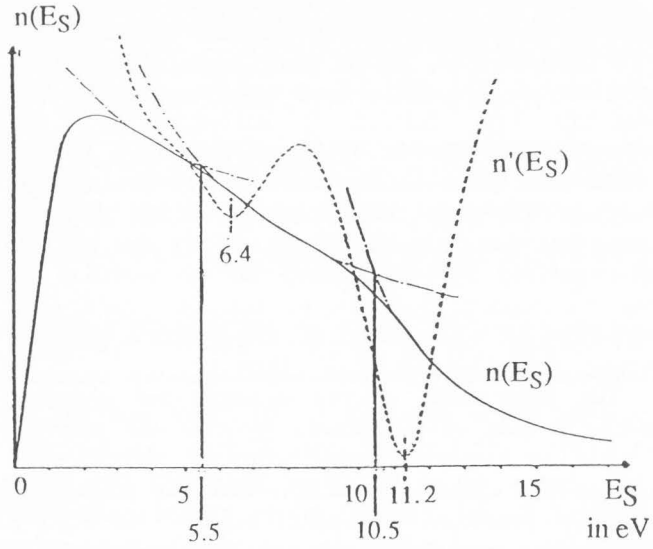

Fig. 3 : Aluminium : True secondary peak n(E_S) and derivative curve n'(E_S) = dn(E_S)/dE_S at E_p=300 eV. Modulation amplitude for n(E_S) : 80 mV peak-to-peak, for dn(E_S)/dE_S : 1V peak-to-peak, (from Pillon et al. (1976)). The high energy part of the true secondary peak can be well described by three power laws (dash-dotted curves). The corresponding boundary energy values are 5.5 and 10.5 eV.

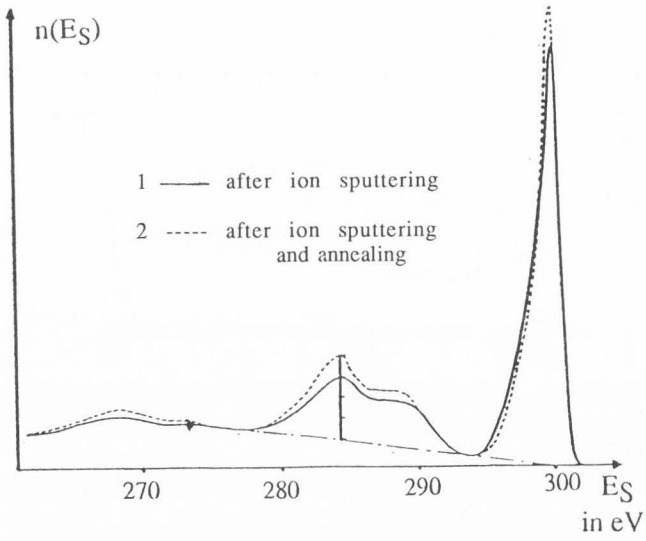

Fig. 4 : Aluminium : Energy loss spectrum at E_p=300 eV. Modulation amplitude : 0.2 V peak-to-peak, (from Pillon et al. (1976)).

cycle of the cleaning process, the Auger spectrum was still typical of an oxidized surface, but after numerous cycles, an Auger spectrum characteristic from clean aluminium was obtained. During the cleaning, the width of the true secondary peak increased and two features (most clearly visible on the derivative mode spectrum) appeared at about 10.6 and 15.4 eV above the Fermi level (see Fig.3). If the localization of these features was not very well resolved on the energy distribution n(E_S), the high energy part of the true secondary peak could however be separated into three energy ranges in each of which the experimental curve was rather well described by a power law (see Fig.3). The energies of the boundary values of these energy ranges measured from the vacuum level were found being E_1=5.5 eV and E_2= 10.5 eV. Also, breaks in the slope were pointed out in the derivative curve by the presence of the negative peaks at E'_1 = 6.4 eV and E'_2 = 11.2 eV. The true secondary peak structures were interpreted as being due to an emission of electrons excited from the valence band by an energy transfer during the decay of a surface or bulk plasmon. Different observations strengthened this interpretation, as for instance, the simultaneous appearance of characteristic plasmon energy losses in the electron energy loss spectrum (see Fig.4) and the close agreement between the experimental and the theoretical values of the plasmon energies.

Similar results were obtained quite simultaneously by Everhart *et al.* (1976).

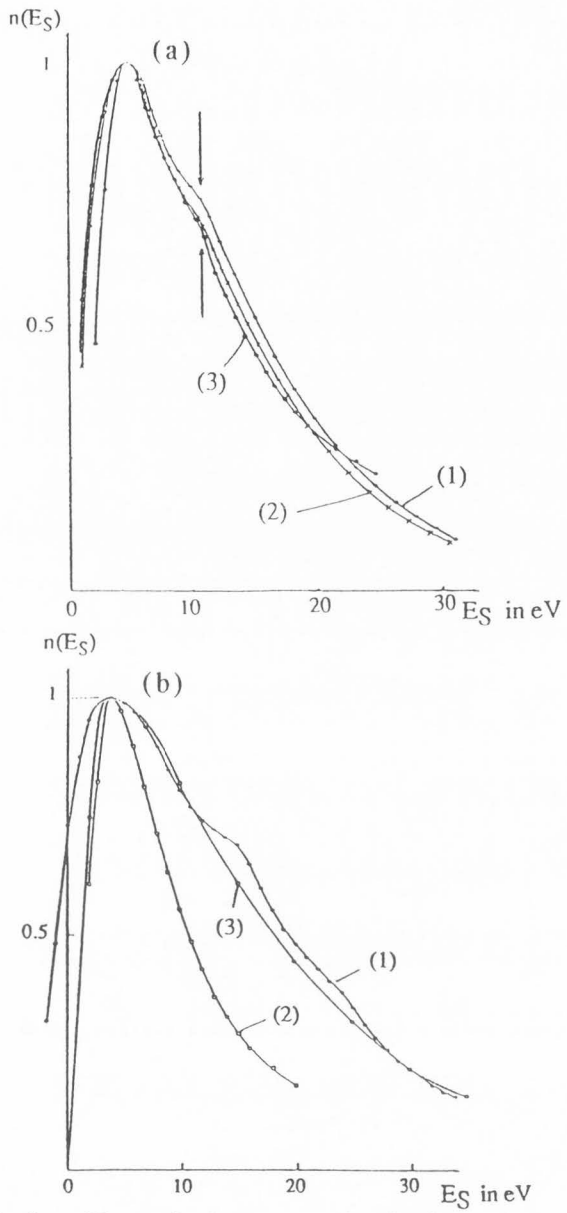

Fig.5 : Theoretical energy distribution of the secondary electrons emitted from noble metals
(a) Cu, (1) Theoretical results (W=11.1eV, E_p= 200eV, R_{min}=1.4Å, λ_{in}=27Å), (2) Theoretical results (W=10.1eV, Ep=200eV, R_{min}=1.4Å, λ= 27Å), (3) Experimental results (Scheibner and Tharpe (1967);
(b) Au (1) Theoretical results (Boltzmann transport equation and constant mfp), (2) Theretical results (Boltzmann transport equation and Ritchie and Ashley's mfp (1965)), Experimental results (Rudberg (1936) (from Cailler (1969). W= $E_F+\Phi$ where E_F is the Fermi level and Φ the work-function of the material, R_{min} is the impact parameter and λ_{in} the total inelastic mean free path.

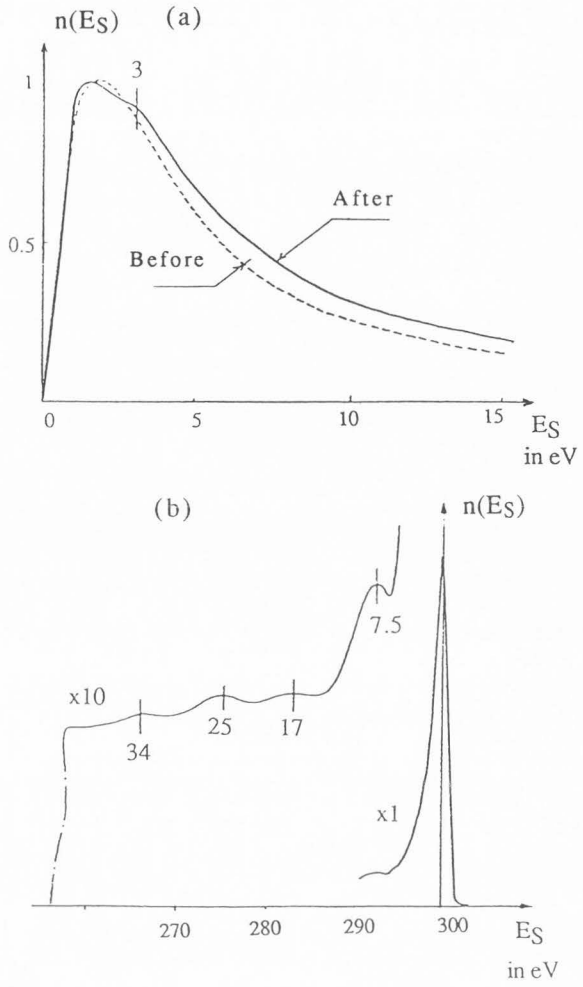

Fig.6 : Silver : (a) The true secondary peak before and after in-situ surface cleaning and (b) the energy loss spectra after cleaning. (From Cailler et al. 1977).

Theoretical evaluations of the contribution of plasmon decay to the secondary electron emission were then given by Ganachaud (1977), Ganachaud and Cailler (1979 a,b) and by Chung and Everhart (1977). However, scattering from the nuclei was neglected in the paper by Chung and Everhart.

Interband transitions

The possibility of the presence of features in the secondary electron peak of noble metals had been theoretically predicted from a comparison between the electron and optical transition probabilities by Cailler (1969) (see Fig. 5). For copper, similar results were obtained by Ganachaud and Cailler (1973) (see also Cailler and Ganachaud (1972)), either through a Boltzmann equation or a Monte-Carlo simulation method.

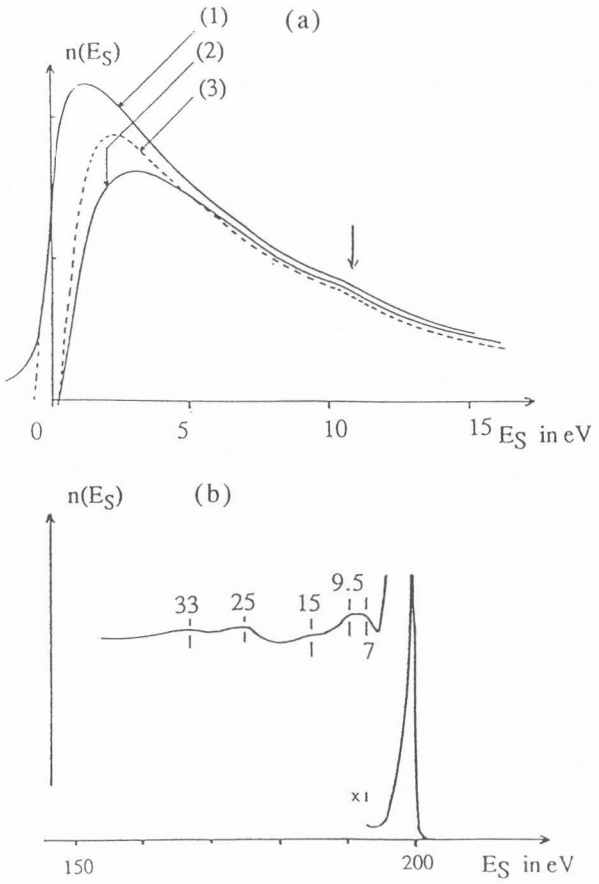

Fig.7 : Gold : (a) The true secondary peak before and after in-situ surface cleaning and annealing (1) polycrystalline Au after annealing (2) polycrystalline Au before annealing (3) [100] single crystal and (b) the energy loss spectra after cleaning. (From Cailler et al. 1977).

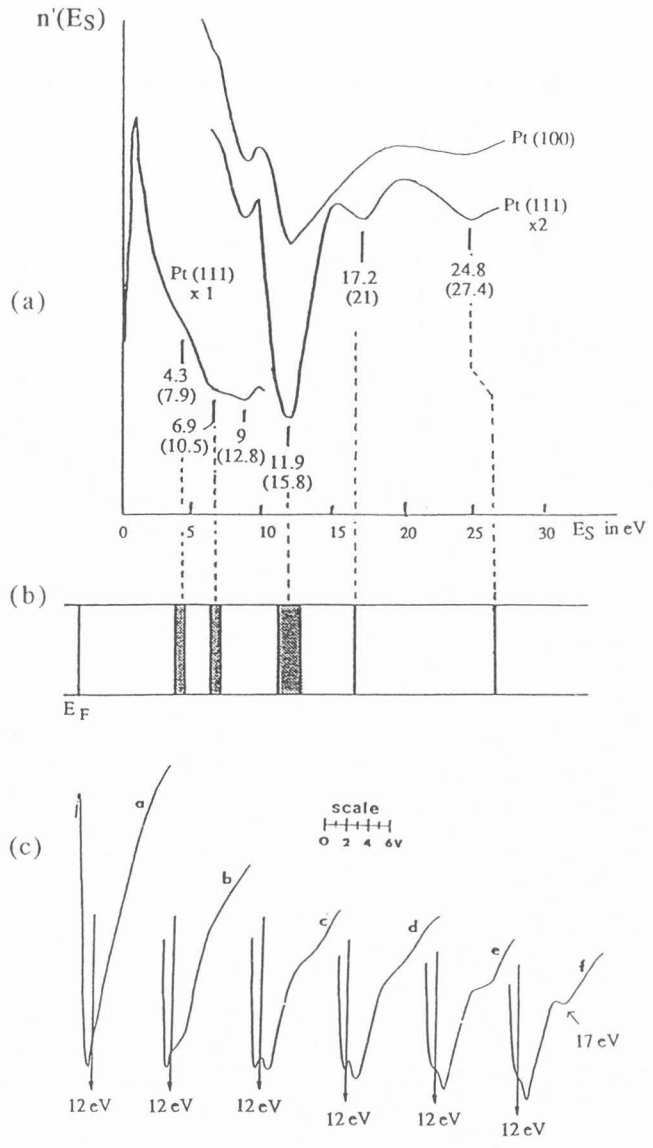

Fig.8 : Secondary electron spectroscopy of platinum surfaces (From Lang (1977)). (a) Secondary electron spectra of Pt (111) and Pt (100). Peaks occur at retarding voltages V_R : 1.6, 3.5, 4.5, 6.5, 12.2 and 20.0 V. The corresponding energies measured with respect to the Fermi level are given in parentheses. (b) Final states for optical transitions (From Seignac and Robin (1972)). (c) Secondary electron spectrum of Pt (100). Evolution of the fine structure of the 12 eV peak and growth of the 17 eV peak as a function of exposure to CO, in Langmuir (L) : (a) 0 L, (b) 1.6 L, (c) 3.4 L, (d) 5.8 L, (e) 7.2 L, (f) 9 L.

Experimental observations were brought in studies performed on graphite by Willis *et al.* (1971a, 1971b, 1974) and interpreted in terms of interband transitions. For noble metals, measurements were performed by Pattinson and Harris (1972) on polycrystalline silver and by Roptin (1975) and Cailler *et al.* (1977) on silver and gold single crystals. For single crystal silver, a fine structure was observed at nearly 7.2 eV above the Fermi level (Fig. 6a) and was correlated with an electron energy loss at 7.5 eV (Fig. 6b) and with optical energy loss measurements. An explanation in terms of interband transition to unoccupied final states was proposed. It had been initially proposed by Smith (1974), in order to explain the rapid appearance of peaks in his photoelectronic energy distributions at growing photon energy. This explanation was also in agreement with band structure calculations performed by Cooper *et al.* (1971), showing an horizontal band at 6.8 eV above the Fermi level along the direction XW of the Brillouin zone. For gold, a fine structure appeared in the secondary peak at about 16 eV above the Fermi level (fig. 7a) and

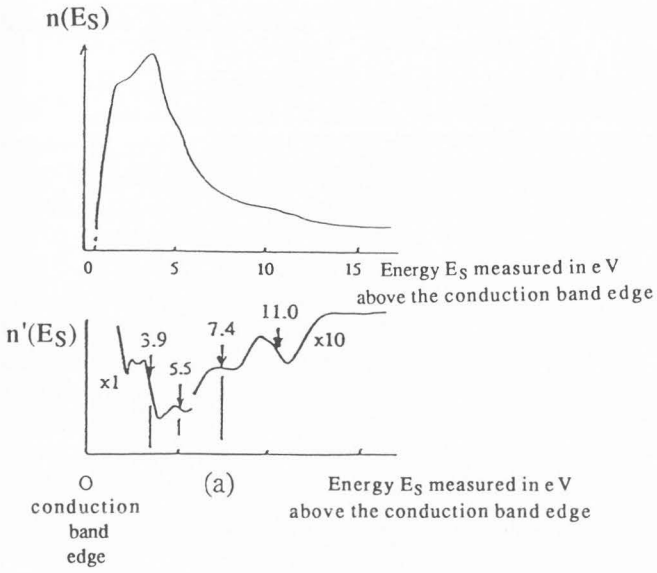

Fig.9(a) : Secondary electron spectroscopy of BaO (From Thomas et al. (1978)). Secondary electron spectrum for BaO at a primary beam energy of 50 eV. Peaks occur at 3.9, 5.5, 7.4 and 11.0 eV (secondary electron energies measured with respect to the conduction band edge).

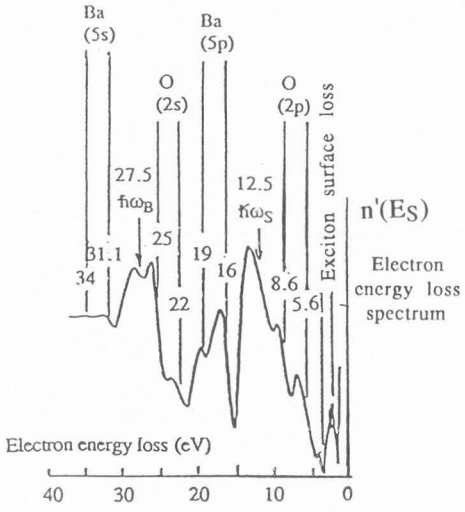

Fig.9(b) : Electron energy loss spectrum of BaO. (From Thomas et al. (1978)). Loss peaks were designated according to the mechanism responsible. The interband transitions were indicated by the involved initial filled level.

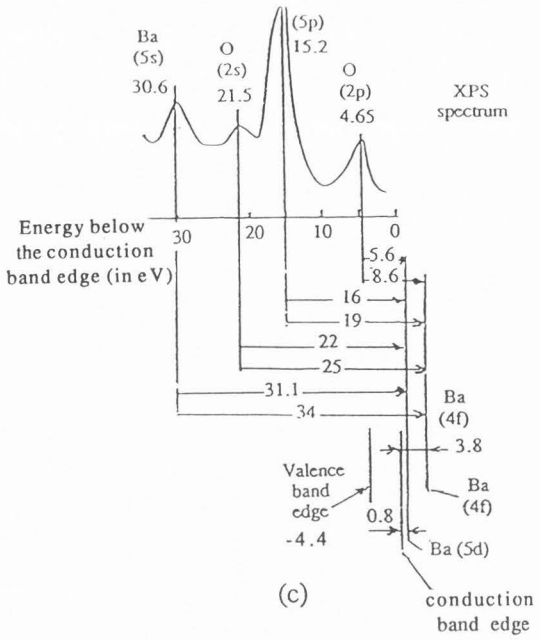

Fig.9(c) : Partial XPS spectrum of BaO and energy diagram for interband transitions (From Thomas et al. (1978)).

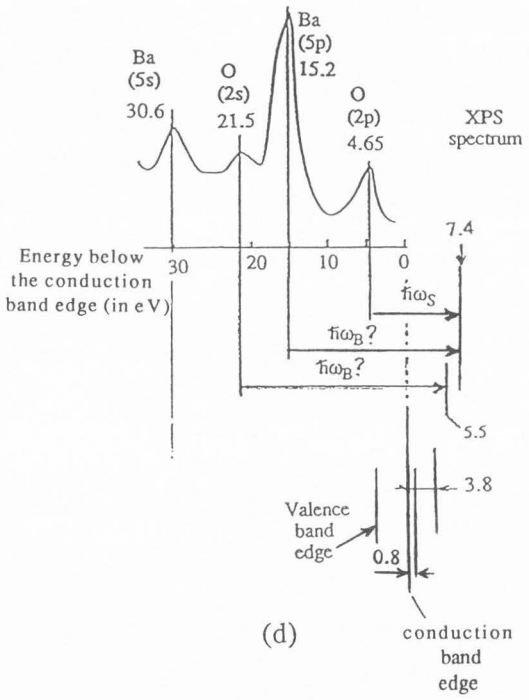

Fig.9(d) : Partial XPS spectrum of BaO and energy diagram for plasmon decay transitions (From Thomas et al. (1978)).

was correlated with a structure at 25 eV in the electron energy loss spectra (Fig.7b). We will return to this question in the section devoted to the doubly differential angle-energy distributions.

Lang (1977) studied the secondary electron emission from platinum with a four-grid retarding field analyzer and observed several peaks in the energy distribution. In spite of the absence of detailed band-structure calculations in the energy

range of interest, he interpreted five of these peaks as arising from transitions to states in the unoccupied f bands (Figs. 8a and 8b). A 6th one, at 21 eV, was sensitive to the surface reconstruction of Pt and was considered as having an unclear origin.

Lang (1977) applied also SES (Secondary electron emission spectroscopy) to the characterization of adsorbate-covered Pt surfaces and to the determination of the amorphous or graphitic nature of carbon surfaces. For that, he introduced CO and C_2H_4 in the chamber and studied the evolution of the SE spectrum, during room temperature adsorption of these gases. He observed that some peaks from Pt were attenuated and that new features could be detected (Fig.8c). These modifications brought informations on the physical origin of fine structures. Lang showed that for a sufficiently long exposure to ethylene, the secondary spectrum of the Pt surface, was very similar to that of a pyrographite surface and he proposed to discriminate between graphitic and amorphous carbon with the help of SES. He showed also that the secondary electron peak, as a whole, was sensitive to the temperature and to the surface disorder.

Thomas *et al.* (1978), have studied by SES, ELS (electron energy loss spectroscopy) and XPS (X-ray photoelectron spectroscopy) the electronic structure in BaO. They found that, at primary beam energies below 100 eV, the secondary electron spectrum was dominated by a peak at 3.9 eV, whereas weaker structures were present at 5.5, 7.4 and 11.0 eV (Fig 9a). The electron energy loss spectrum (Fig.9b) exhibited broad plasmon excitation peaks at 12.5 eV (surface plasmon excitation), 27.5 eV (one-bulk plasmon excitation) and 55 eV (two-bulk plasmon excitation) and many additional structures. In order to correlate the secondary electron and the electron energy loss spectra, the positions of the Ba(5s and 5p) bands and the O(2s and 2p) bands were located by XPS (see Figs. 9c or 9d). Then, the structures at 5.5 and 7.4 eV in the secondary electron spectrum were related to plasmon decay (see Fig. 9d), whereas the structure at 3.9 eV was interpreted as arising from interband transitions to a large peak in the density of states at about 3.8-3.9 eV above the conduction band edge (Fig. 9c). This peak in the density of states was attributed to the unoccupied Ba(4f) states). A second peak in the density of states, located at 0.8 eV, was similarly attributed to the Ba(5d) states. Finally, Thomas *et al.* have concluded that most of secondaries were produced by direct excitation from the O(2s) and Ba(5s and 5p) levels to the unoccupied Ba (4f and 5d) states.

Auger transitions and Fano autoionization emission

These two different mechanisms show however some resemblance. They are both two-step mechanisms. Auger transitions can occur in each atom, at the exception of the first elements of the Mendeleiev table. Autoionization emission was described by Fano and Cooper (1968) in a review paper on the spectral distribution of atomic oscillator strengths. It has been detected for instance in the heavy alkali metals (see Nygaard (1975)) and in the less-than-half full d-shell transition metals. In this latter case, the process was associated with the existence of important correlation effects in the d-bands. Indeed, such important correlation effects are needed to produce autoionization.

A clear description of autoionization emission, can be found in Cornaz *et al.* (1987), for instance. For the sake of clarity, we will reproduce it in what follows. In the first step of both mechanisms (Fano and Auger emissions), a primary electron interacts with an atom and transfers a part of its energy by exciting a core electron of the target atom. In an Auger mechanism, the primary and the excited electrons acquire energies well above the Fermi level, so that the atom is left ionized. If for instance, its initial configuration is np^6nd^z where z is the occupancy number of the d-shell in the neutral atom, its intermediate configuration after the first step is np^5nd^z. In the first step of an autoionization process, either the excited electron or the primary one acquires an energy just above the Fermi level, so that its kinetic energy is too low for it to escape from the vicinity of the atom. In that case, the atom is in the configuration $np^5nd^zd^*$ at the end of the first step, where the electron in the excited state is described by d*.

In both cases, the atom is left excited with a np-hole, so that a nd electron will jump to the vacant np state, in order for the atom to return to a minimum energy state. The energy in excess will be taken by an electron of the same nd band, which will be ejected from the atom. Then, for an Auger transition, the final state of the atom will be np^6nd^{z-2}, whereas for an autoionization emission, it will be np^6nd^{z-1}. According to Fano, the detailed shape of such an excitation is determined by the resonant interaction between the nd^zd^* configurations and the continuum f levels.

Cornaz *et al.* (1987) measured the SES and the EELS from vanadium (see Fig. 10a). In the EELS

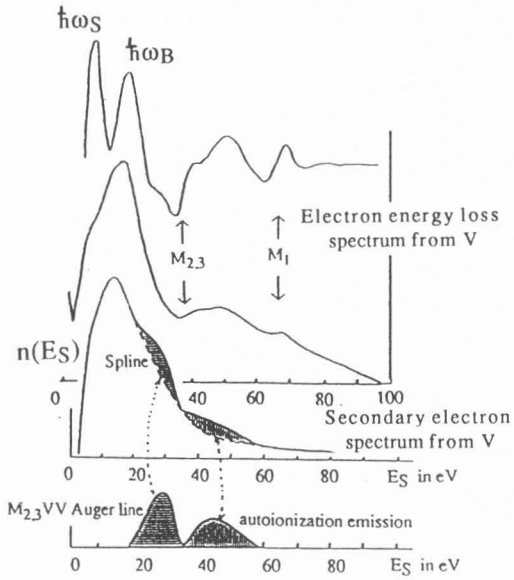

Fig.10(a) : Electron energy loss and secondary electron spectra from vanadium (From Cornaz et al. (1987)).

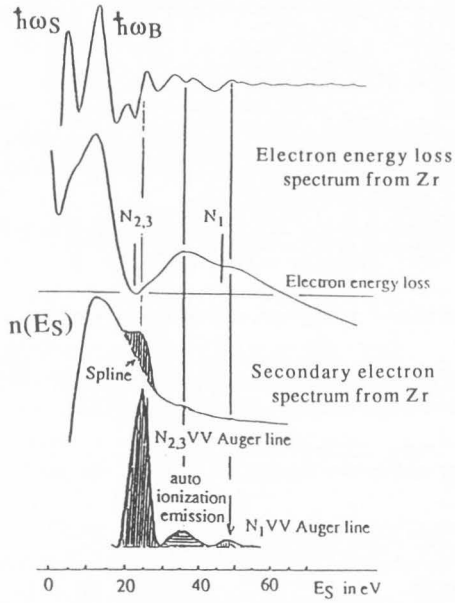

Fig.10(b) : Electron energy loss and secondary electron spectra from zirconium (From Erbudak et al. (1987) and from Aebi et al. (1987))

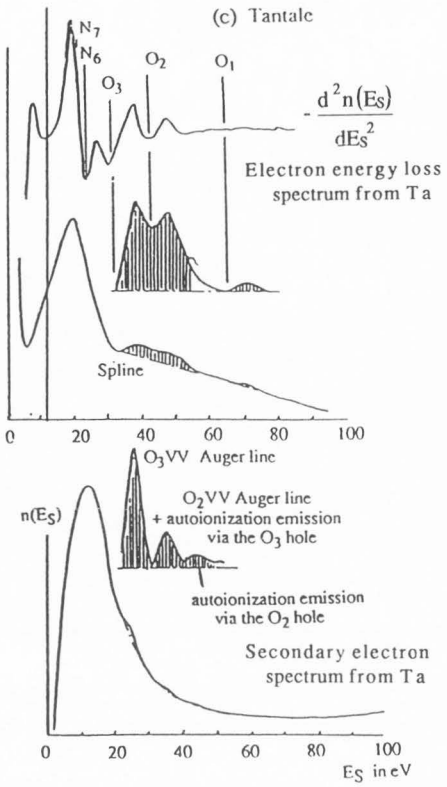

Fig.10(c) : Electron energy loss and secondary electron spectra from tantale (From Cornaz et al. (1987)).

spectrum they observed two structures at 10.0 and 21.0 eV, representing the plasmon losses. A peak at 32.0 eV was also detected and attributed to a higher-order plasmon loss. The onset of the 3p-3d excitation appeared at an energy of 37.1 eV which is the bottom of the $3p_{1/2,3/2}$ core levels. The transition reaches its maximum at around 50 eV and stretches as far as 60 eV. In this energy range, a fine structure was resolved at 41 eV in the second derivative mode. At 66.0 eV, the dipole-forbidden 3s-3d transition (M_1) could be observed. To explain the origin of this transition, Cornaz et al. (1987) performed a calculation by using an analytic function f(E), given by Dietz *et al.* (1974) to describe the Fano autoionization emission (In this function, a summation is made over the final-state multiplets). They were able to show that the calculated results using the atomic data were in good agreement with the experimental curve and, as a consequence, that the discrete final state multiplets interacted with the continuum and that the np-nd (here 3p-3d) excitations were of atomic character.

In the spectrum of secondary electrons, the $M_{2,3}VV$ Auger emission was identified at 28.0 eV and the autoionization emission appeared with its maximum intensity at 44.5 eV and nearly stretched over an energy region of 20 eV. The excitation and emission spectra obtained from a V(110) surface were identical with those for V(100), excluding an effect of the orientation of the surface on the observations.

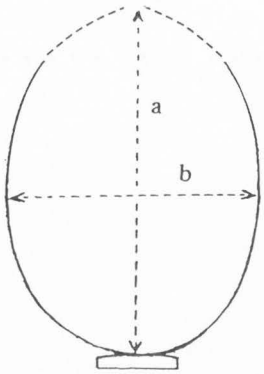

Fig.11 : Eccentricity parameter (Jahrreiss and Oppel (1972))

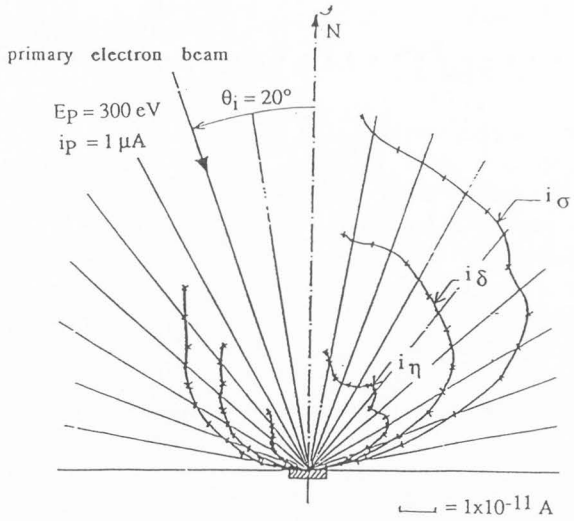

Fig.12 : Angular distributions of the true secondary (i_δ), the inelastically backscattered primary (i_η) and the total (i_σ) electron beams from a gold (111) single crystal target. The primary energy was of 300 eV and the incidence angle of 20°. Ref. Cailler et al. (1977).

Similar results were observed in other transition metals (Figs. 10b and 10c). For instance in the secondary electron peak from tantalum, three main structures were identified at 25.2, 34.5, and 44.3 eV. The two structures at 25.2 and 34.5 eV were assigned to the O_3VV and O_2VV Auger transitions and the structure at around 44.3 eV was interpreted as belonging to the autoionization emission related to the O_2 hole. The O_3 hole autoionization emission should appear at around 35 eV, that is in coincidence with the O_2VV Auger line. The small intensity of the autoionization peak indicates that the atomic character of the 5p-5d transition is less than in the 3d and 4d transition metals.

Aebi *et al.* (1987), Erbudak *et al.* (1987) and Palacio *et al.* (1987), proceeded to similar studies on Y, Zr, Nb and Mo. They studied also the effect on the SES and EELS spectra, of an oxidation of the Zr surface. For clean Zr, the dominant structure in the SE spectrum was the $N_{2,3}N_{4,5}N_{4,5}$ transition, with its maximum at 24.3 eV. The $N_1N_2N_{4,5}$ and $N_1N_3N_{4,5}$ Auger transitions could be resolved in the second derivative mode. The autoionization emission appeared between 29.0 and 43.7 eV and the $N_1N_{4,5}N_{4,5}$ Auger emission was peaked at 47.8 eV.

Under oxygen adsorption on the Zr surface, there are important modifications in the $N_{2,3}N_{4,5}N_{4,5}$, $N_1N_2N_{4,5}$ and $N_1N_3N_{4,5}$ Auger transitions which were interpreted as resulting from an electron transfer from metal to oxygen reducing the occupancy of the Zr 4d band. On the contrary, no important change was reported in the energy and the intensity of the autoionization emission peak.

2) Angular distributions

The angular distributions of secondary electrons were often reported to follow typically a cosine law. This question was studied by several authors. Jahrreiss and Oppel (1972), studied angular distributions of the true secondary and the backscattered primary electrons from thin films of Al and Au. Measurements were performed in forward and backward directions with primary energies in the interval 1 to 20 keV and with normal or oblique incidence of the primaries. In addition, the angular distributions of secondary emission from bulk samples of Al, Cu, Ag, Au, In, Ni, Ta and W samples were investigated. For the true secondary electrons they found only very small deviations from the cosine distribution in transmission as well as in backemission. An exemple of angular distribution is shown in their paper for a self-supported thin film of gold. The thickness of the film was of 50 nm and the primary energy of 10 keV. On the contrary, for the backscattered primary electrons, they observed several characteristic differences between the measured curves and the cosine distribution. The overall shape of these distributions, drawn in a polar plot, were characterized by an eccentricity parameter χ = a/b (see Fig. 11) where a is the length of the distribution curve in the surface normal direction and b the larger length of the same curve in a direction parallel to the surface. Jahrreiss and Oppel (1972) Oppel and Jahrreiss (1972) have compared angular distributions of secondary and backscattered primary electrons

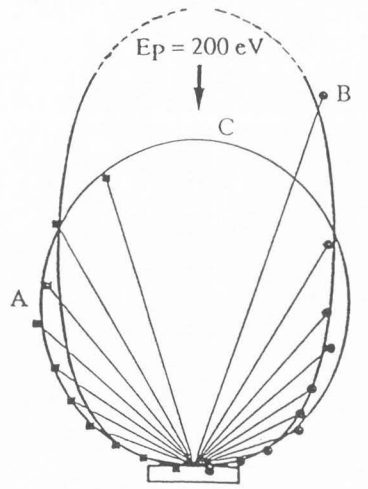

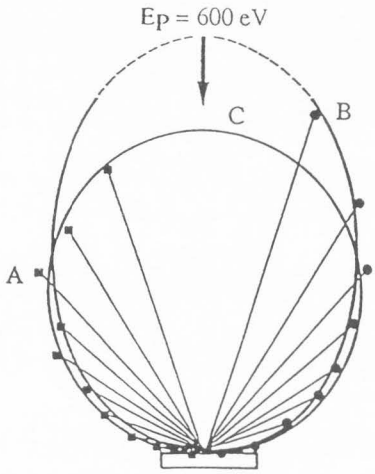

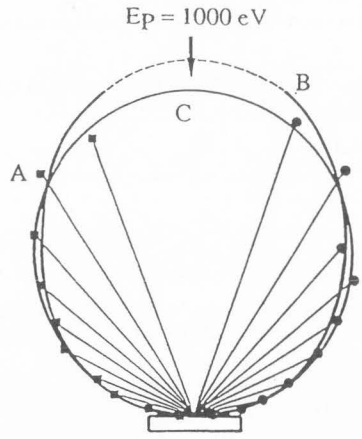

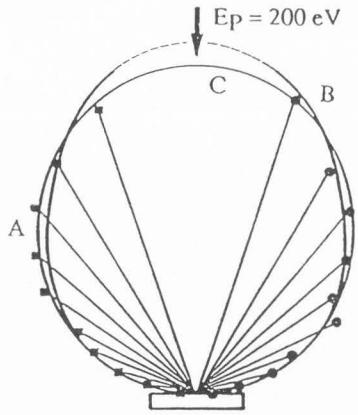

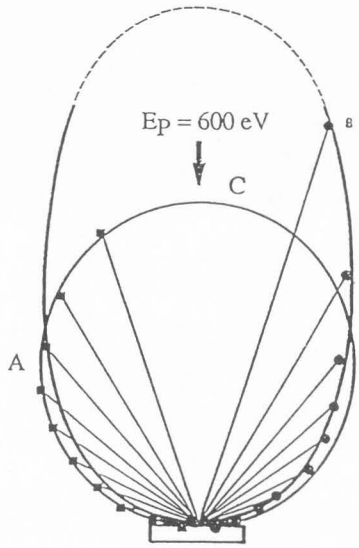

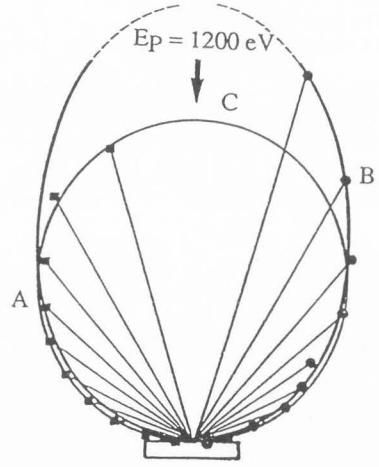

Fig.13 : Simulated angular distribution from copper (Ganachaud (1977)) A : True secondary, B : Inelastically backscattered, C : cosine law.

Fig.14 : Simulated angular distributions from gold (Ganachaud (1977)), A : True secondary, B : Inelastically backscattered, C : cosine law.

from self-supported thin films as well as on polycrystalline and single crystalline samples in Al and Au. Hornemann and Jahrreiss (1976), measured angular distributions on evaporated layers of Ag, Sb, Ce, Pt, Au, Pb and Bi of backscattered primary electrons and were able to discriminate between electrons which have undergone single and multiple scattering. Bronshtein *et al.* (1972)

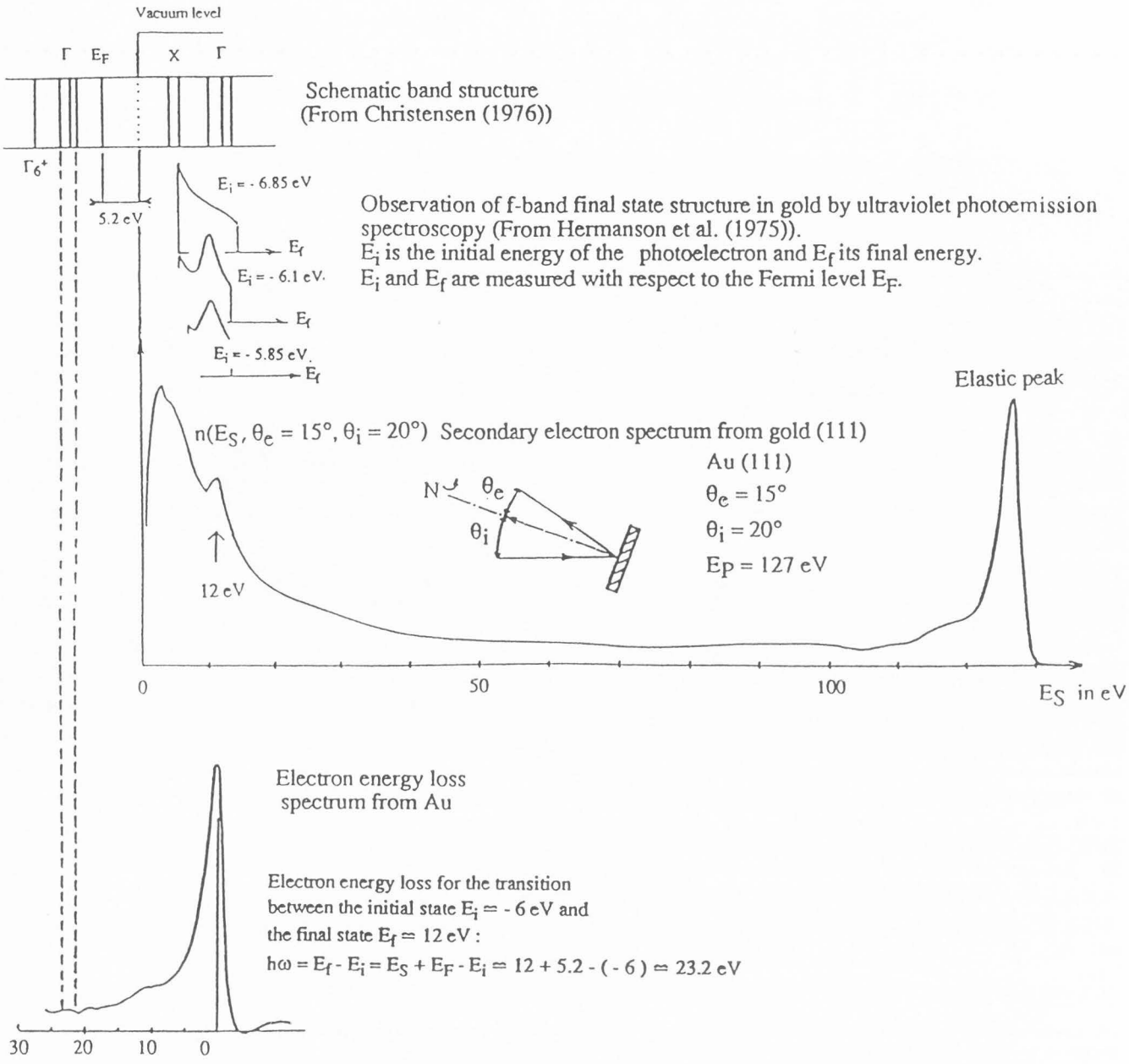

Fig.15 : A complete energy distribution of the electrons emitted from a gold [111] single crystal, as measured with a moving Faraday cage in the (00) spot (From Cailler et al. (1977)). Results obtained for the electron energy loss spectrum (Cailler et al.(1977)), the UPS emission (Hermanson et al. (1975)) and the band structure calculations (Christensen (1976)) are also shown for comparison.

reported measurements on the angular distribution, for different targets, different primary energies and different incidence angle. Cailler *et al.* (1977) measured with a rotating Faraday cage, the angular distributions of the true secondary, the inelastically backscattered primary electrons and the total emitted current. Fig. 12 shows the results obtained on an Au (111) single crystal target, for a primary energy of 300 eV and an incidence angle of 20°. The true secondary electron exhibited more or less a cosine distribution, whereas the inelastic backscattered primary electron distribution revealed strong anisotropies. These anisotropies were still perceptible on the total current, but with a clearly lower strength.

Some angular distributions obtained for Cu and

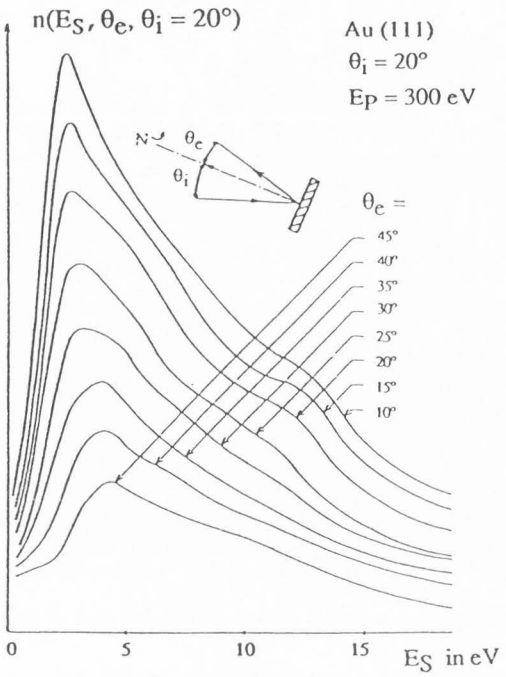

Fig.16 : Emergence angle dependence of the true secondary peak from a gold [111] single crystal, as measured with a moving Faraday cage. From Cailler et al. (1977).

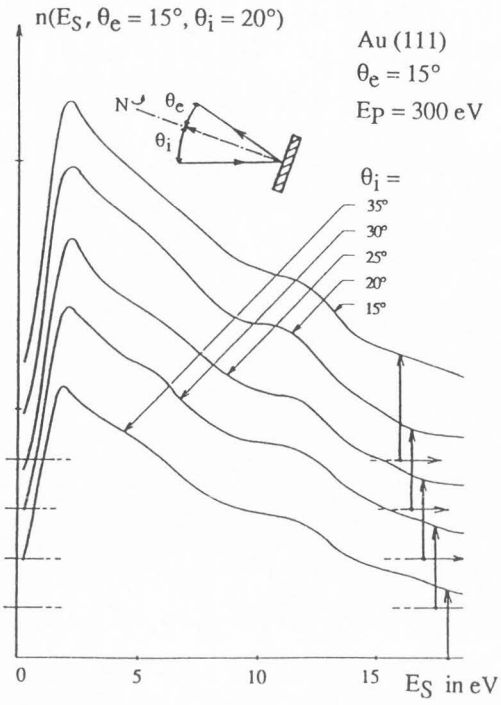

Fig.17 : Incidence angle dependence of the true secondary peak from a gold [111] single crystal, as measured with a moving Faraday cage. From Cailler et al. (1977).

Au, by Ganachaud (1977) with a Monte-Carlo simulation model on a computer are shown in Figs. 13 and 14. In such models, the coherent diffraction effects were not taken into account, so that crystalline effects could not be included. In every case, the angular distribution of the true secondary electrons followed a cosine law. A completely different evolution with the primary energy was observed for the backscattered primary electron distribution. For Cu and at low energy, a high intensity was calculated in the normal direction to the surface. This anisotropy was decreasing with increasing primary energy. At 1 keV, the calculated eccentricity ($\chi_{cal} \simeq 1.1$) was found in satisfactory agreement with measurement results ($\chi_{meas} \simeq 1.1$) by Jahrreiss and Oppel (1972). For Au the eccentricity was very small at 200 eV. On the contrary, it was high at 600 eV, but presented a slight decrease when the primary energy was increased to 1200 eV. An explanation in terms of relative values of the inelastic, the elastic and the elastic backscattering mean free paths was proposed.

3) Angle-energy distributions

An angle-energy resolved secondary electron distribution was measured by Cailler *et al.* (1977) with a moving Faraday cage rotating around the sample. The ambient magnetic field was compensated by Helmholtz coils and its residual value was measured with a Hall probe. The horizontal component was found to be of 0.15 G and the vertical one of 0.3 G. A LEED diagram was taken for a primary energy of 127 eV and an incidence angle of 20°. In the (00) spot direction (the corresponding measured emergence angle was 15°) the LEED diagram had an amplitude maximum. Its intensity was rapidly vanishing when the Faraday cage was rotated by a few degrees from its optimal value 15°). The energy distribution obtained in this (00) spot direction was shown to exhibit a very sharp fine structure at about 17 eV above the Fermi level (see Fig. 15). It was shown to be correlated with a structure at 25 eV in the electron energy loss spectra. A comparison with results of UPS measurements, obtained in a constant-initial-state energy spectrum mode by Hermanson *et al.* (1975), was performed. In the UPS spectra, there were strong structures, which were associated with atomic transitions from occupied d levels located between -4.35 and -6.85 eV below the Fermi level, to unoccupied f-levels located between 14 and 18 eV above this Fermi level. This explanation was supported by a comparison with band structure calculations by

Christensen (1976). The similitude in the transition energies and in the final state energy levels, allowed us to consider that Hermanson's interpretation could be applied to our results. An additional proof was found in the fact that the structures in the UPS and SE spectra had the same width in energy that the f-bands. The apparent amplitude of this structure was clearly decreased when the Faraday cage was rotated (Fig.16). Furthermore, a second less intense structure (see Figs.15 and 16) could be observed near a kinetic energy of 5 to 6 eV, that is about 11 eV above the Fermi level, in correspondence with similar observations by Hermanson *et al.* and with results of band-structure calculations. All these structures were shown to be independent of the incidence angle (Fig. 17).

Much more detailed angle-energy distributions were given by Willis and Feuerbacher (1975), Willis *et al.* (1976, 1977), Willis and Christensen(1978), Christensen and Willis (1978, 1979). For instance, Willis and Christensen (1978) have measured angle-resolved energy-distribution of secondary-electron emission from (100), (110), and (111) tungsten surfaces by using a LEED-Auger 130°-sector cylindrical electrostatic analyzer with an angular resolution of less than 0.1°. The first grid of the LEED optics was grounded in order to provide a hemispherical region free from electrostatic field around the sample.

The magnetic fields in the scattering and analyzing region were reduced below 10 mG by enclosing this region with Mumetal shells. The target crystal could be rotated about an axis of its surface (varying polar angle θ) and about an axis normal to its surface (varying azimuthal angle ϕ). The primary electron beam was incident at an angle of 45° to the crystal surface normal and had a beam-energy spread of around 0.3 eV at the beam energy 100 eV used in the experiments.

Angle-resolved energy-distribution spectra of secondary electrons emitted normally to W crystal (100), (110), and (111) faces, were measured for an incidence angle of 45°. They showed clearly resolved minima, indicative of an energy gap along the three principal-symmetry lines ΓH (Δ <100>), ΓN (Σ <110>) and ΓP (Λ <111>) of the Brillouin zone (Fig.18). These minima extended from 2.5 to 4.5 eV, 0.8 to 5.4 eV, and 3.2 to 4.4 eV, respectively. Other fine structures appeared in the lower secondary electron part of spectra obtained on the (100) face (at around 2.5, 5.0 and 11 eV) and on the (111) face (at 3 eV). They were superimposed on a high intensity background and their width was increasing with the secondary

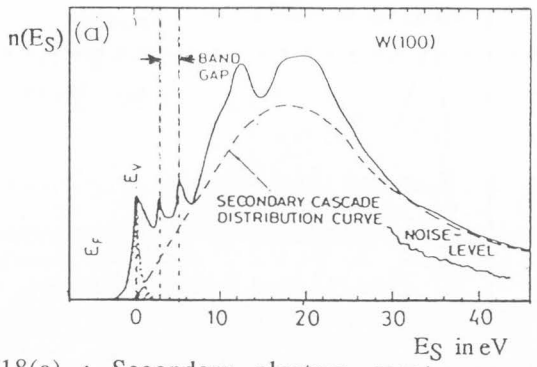

Fig.18(a) : Secondary electron spectra measured normally to W(100) surface. From Willis and Christensen (1978).

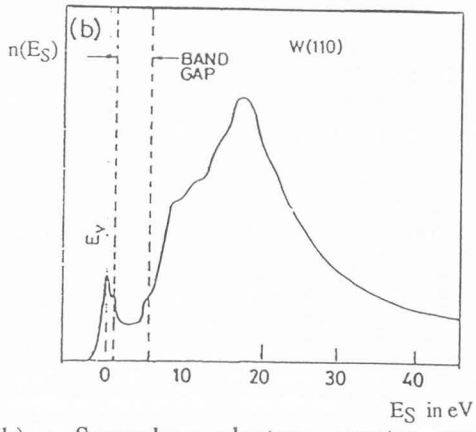

Fig.18(b) : Secondary electron spectra measured normally to W(110) surface. From Willis and Christensen (1978).

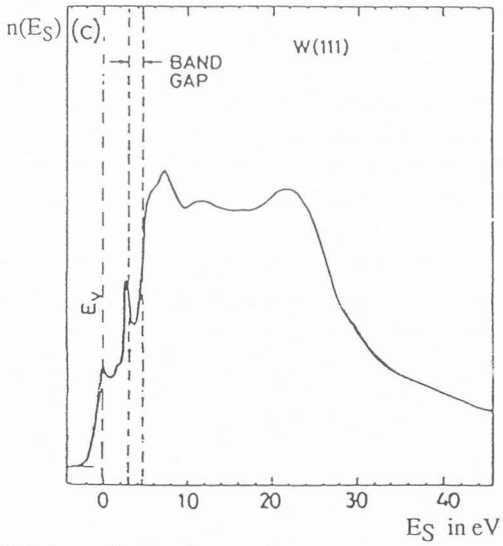

Fig.18(c) : Secondary electron spectra measured normally to W(111) surface. From Willis and Christensen (1978).

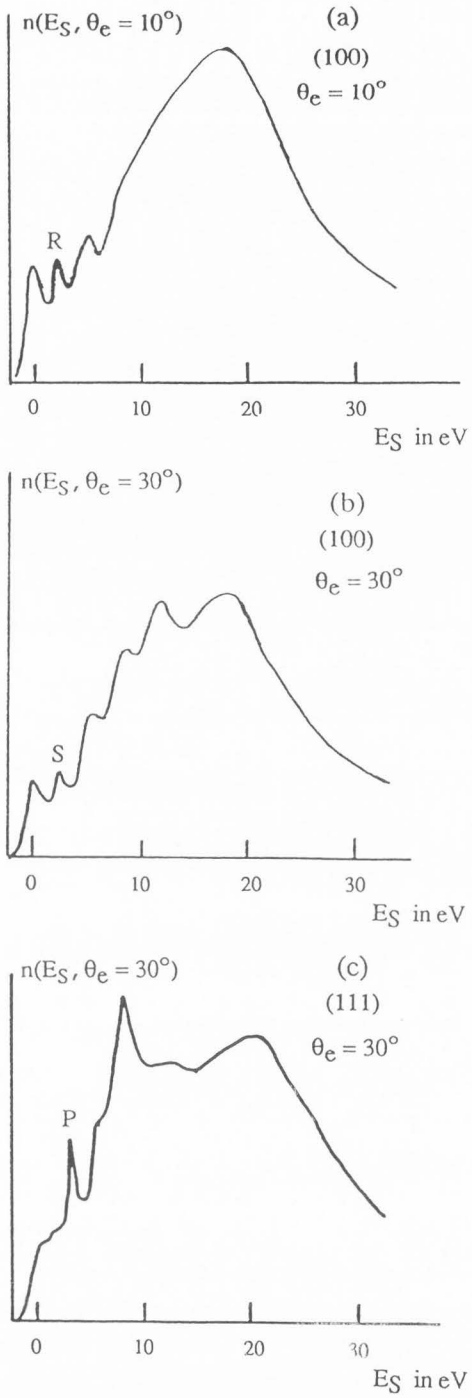

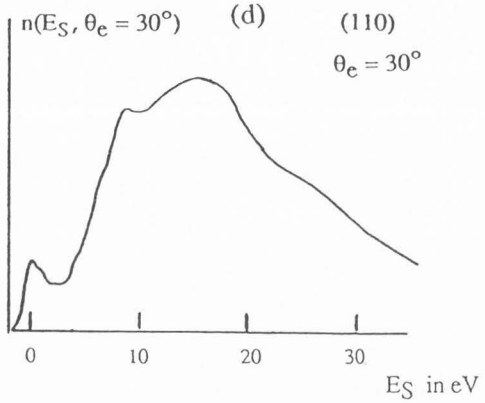

Fig.19 : Angle-dependent secondary electron emission spectra showing the spectral intensity for (100), (111) and (110) tungsten surfaces and for given values of the emergence polar angle θ_e. These values of the emergence angle were chosen in order to exhibit the anomalies P, R and S. (a) W(100), θ_e=10°, (b) W(100), θ_e=30°, (c) W(111), θ_e=30°, (d) W(110), θ_e=30°. In this latter case there is no apparent anomaly in the angle-resolved SEE spectrum. From Willis and Christensen (1978).

electron energy. Such fine-structures appeared to be absent in the case of the W(110) spectrum. In order to make a more detailed comparison with the theoretical density of bulk states profiles, the background was very roughly subtracted from the experimental secondary electron spectra. A good agreement was reached in the case of the (100) and (110) faces particularly at lower energies. The agreement was not so good for the (111) face, however even in this case, there was a good correlation between the theoretical band gap of the bulk density of states of crystals and minima in the secondary electron spectrum.

The angular dependence of the SEE spectra from (100), (110), and (111) tungsten surfaces was studied as a function of the emergence polar angle θ_e (in the range 0 to 70°) along azimuthal directions ϕ. The experimental spectra and theoretical bulk single-particle densities of states were found to show a good overall agreement. Secondary-electron yield results might be represented as the sum of two contributions, one from the bulk and the other from the surface.

However, three "anomalies" were apparent in the angle-resolved SEE spectra (see Fig. 19) :

1) a peak labeled P in the W(111) spectra
2) a peak labeled R in the θ_e=10° W(100) spectra and
3) a peak labeled S in the $10<\theta_e<70°$ W(100) spectra .

These features could not be explained as being due to any bulk density of states contributions and were considered as indicative of a need to include surface wave-matching arguments in the analysis of secondary electron emission spectra (see Fig.20). Such a wave-matching was expected to affect mainly the relative intensities of the fine structures.

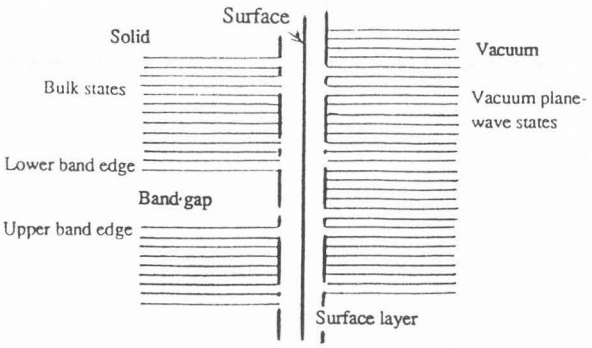

Fig. 20 a

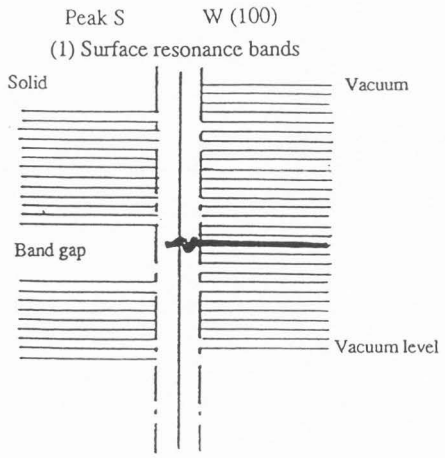

Fig. 20 b

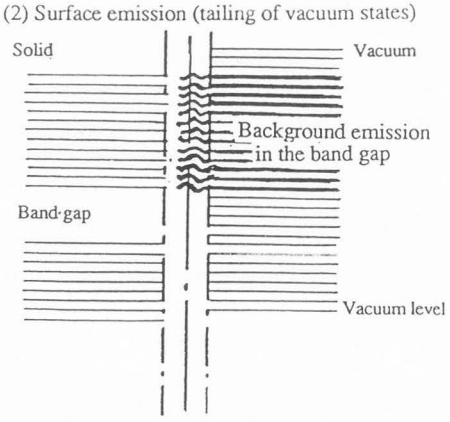

Fig. 20 c

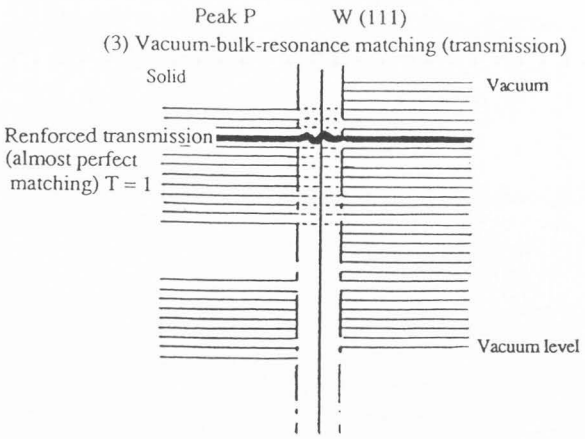

Fig. 20 d

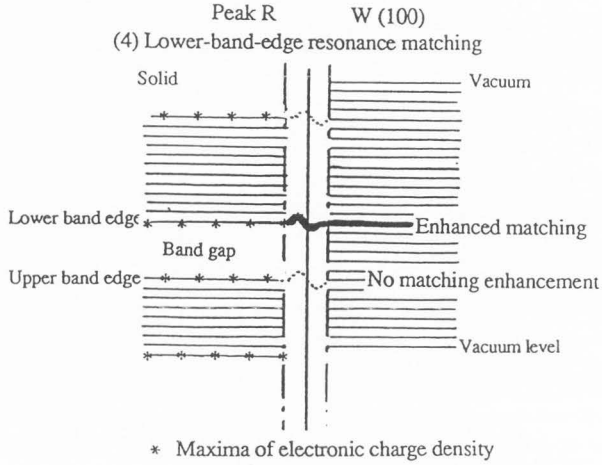

Fig. 20 e

Fig.20 : Schematic diagrams of the mechanisms pro-posed by Willis and Christensen to account for the background emission in the band gap and the anomalies P, R and S in the angle-dependent secondary electron emission spectra from tungsten. (a) One-dimensional schematic illustration of final-state electronic wave-functions in vacuum and the bulk of the solid, (b) Surface resonance bands, (c) Surface emission (tailing of vacuum states), (d) Vacuum-bulk-resonance matching (transmission), (e) Lower -band-edge resonance matching

The feature S was identified with emission due to an intrinsic surface resonance effect associated with a band of surface states (resonances) arising in the surface Brillouin zone, inside the energy gap between the bulk states. These surface states (resonances) are a common feature of the W(100) surface and were also observed in the case of ordered monolayers of adsorbate gases on this surface. These latter adsorbate-induced resonances disappeared when the adsorbate "superlattice" was becoming disordered, under thermal treatment.

The background emission in the band gap was attributed to surface emission. Indeed, for energies above the vacuum level, the continuum of plane-wave vacuum states are always able to penetrate a short distance into the solid. This tailing of the vacuum wave functions into the surface

region was considered as matching at every point in the surface unit cell the waves emitted from surface excited atoms and the vacuum plane wave states.

The peak P was connected with an enhanced emission arising from the quantum-mechanical (wave-matching) properties of the transmission probability function $T(E,k_{//})$. Indeed, the transmission of current through the surface is considerably enhanced when the bulk emitting state has a group velocity which is exactly equal to that of the emitted electron in vacuum. Under these particular conditions, the current carried by the Bloch waves incident on the surface is conserved and the transmission probability amplitude coefficient has a maximum value. This structure is particularly sensitive to surface contamination.

Peak R at θ_e=10° from the W(100) face, represents an example of a resonance matching effect called by Willis and Christensen "the lower-band-edge resonance matching". This sharp resonance which is the result of constructive interferences between component waves of comparable magnitude exists at the extremities of energy band gaps on the zone boundaries. On these boundaries, the component plane-waves travelling in opposite directions combine to form standing waves. The standing wave associated with the lower-band-edge presents an amplitude maximum at the outermost atomic layer, thereby providing a local source of current. In contrast, the upper edge of the gap represents a minimum in the wave amplitude at the surface. Surface emission arising from the tailing of the plane vacuum state into the solid could be enhanced by the lower-edge resonance. As a result of measurements, the P fine structure was effectively shown to be sharply peaked at the lower band edge. A similar situation could exist for peak P for emission at θ_e=20° from the W(111) face, but it was considered that here the effect was less clear due to the simultaneous incidence of the above described vacuum bulk resonance matching mechanism. Again, these features are sensitive to surface perfection and contamination effects.

Schäfer *et al.* (1981) have measured the angular resolved energy distribution of true secondary electrons emitted normal to a clean W (100) surface with a 180° spherical deflector analyzer. Their results obtained for an incidence angle of 45° presented an overall agreement in the energetic positions of the fine structure features with those of Willis and Christensen (1978), but differed significantly as regards the general shape of the true secondary peak. Indeed, contrarily to

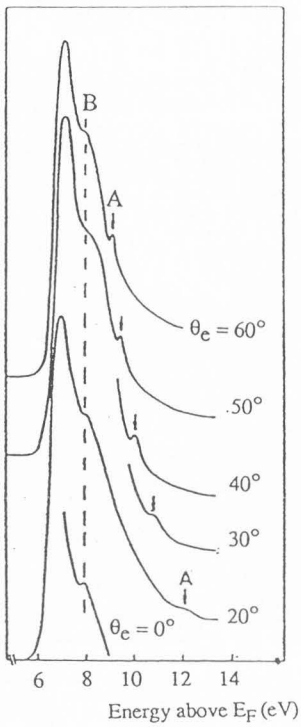

Fig.21 : Electron secondary emission spectra observed at different emergence polar angles θ_e in the ΓXWK azimuth for the case of a copper sample covered with chlore. From Zimmer et al. (1984).

those of Willis and Christensen (1978), all the curves obtained by Schäfer *et al.* exhibited a general shape which was close to that obtained for the smooth angle-integrated energy distribution curve. This smooth background was approximated by an analytical function $B(E) = E/[(E+\phi)(E+b)^y]$ with ϕ = 4.55 eV, b= 2.7 eV and y = 1.88, and the experimental data for the angular resolved energy distribution were divided by B(E). The results so obtained by Schäfer *et al.* were in excellent agreement with reflection coefficient measurements and theoretical results deduced from the Feder and Pendry theory (1978).

The origin of the differences between the Willis and Christensen (1978) results and their own measurements was not discussed in details by Schäfer *et al.* However, in their paper, it is strongly suggested that these differences could find their origin, at least partially, in the transmission functions of the analyzing systems.

Recently, Zimmer *et al.* (1984) measured angle-resolved electron energy distribution curves from Cu(001) c (2x2)-Cl by photoelectron spectroscopy

and SES. The resolution parameters were typically of ± 1° and of 60 to 100 meV. The curves were taken at different polar angles θ, both in the ΓXWK and the ΓXUL planes of the Brillouin zone of Cu. A peak observed at kinetic energy E_{kin} with respect to the vacuum level E_v and emission angle θ with respect to the surface normal was associated with the vacuum wave-vector component :

$$k_{//} = \sin\theta \, [(2m/\hbar^2) E_{kin}]^{1/2} \qquad (4)$$

whereas $k_{\perp}$ remained undetermined. Two fine structures appeared in the SES spectrum, when copper was covered with chlore. Zimmer *et al.* labelled them A and B in the ΓXWK plane (cf. Fig. 21) and C and D in the ΓXUL plane. Only feature B was observed in spectra taken from the clean Cu(001) substrate. Therefore, the appearance of bands A, C and D had to be correlated with the ordered overlayer mesh. Contrarily to the other ones, the feature B was only very weakly dispersed in energy. It was considered by Zimmer *et al.*, as being due to direct secondary electron emission from the substrate. The features A, C and D could not be explained as contributions from Auger transitions nor as a secondary electron emission arising from a transition to empty chlorine-derived bands. According to Zimmer *et al.* (1984), band D could only be interpreted in terms of substrate band emission followed by a surface umklapp process induced by the adsorbate. On the contrary, the bands A and C might also well be explained by a surface resonance emission induced by the adsorbate.

4) Secondary electron emission crystal current method (SEECC)

This technique which is not a spectroscopic one, was proposed by Argile *et al.* (1984), to study metal monolayer adsorption by measuring changes in the secondary electron emission crystal current. The crystal current i_c is equal to $(\sigma-1)\, i_p$, where σ is the total secondary emission coefficient (including reflected primaries) and i_p is the primary electron current. The principle of this type of measurement is well known and it is used qualitatively in scanning secondary electron emission spectroscopy. But, Argile *et al.* were the first to proceed to a detailed quantitative comparison of i_c variations with Auger electron spectroscopy (AES), LEED and work function measurements. Results obtained on Cu (111) and Cu (100) single-crystal substrates have shown that the adsorption of monolayer quantities of lead could be readily followed by the crystal current measurements and that the precision was higher than that attained by AES. They were able also to detect changes in adsorbed layer structures that were much less apparent from the AES data.

As mentionned by Argile *et al.*, the most obvious explanation for the observed variations of the crystal current is work function changes in the surface barrier during adsorption. Argile *et al.* have shown that changes in yield are not necessarily related to work function changes. For instance, for the (111) face, the most significant difference is observed when the monolayer coverage is exceeded. Indeed, in that case, the work function attains a plateau whereas the crystal current decreases sharply. For the (100) face, a sharp maximum in the crystal current followed by a drop was observed for a coverage of 2/3, which could not be correlated with any variations in the other measurements.

Argile *et al.* have shown that these changes in the crystal current should be correlated with structural changes in the ad-layer. The crystallinity of the surface layers may have an influence through electron scattering and diffraction at different stages: the partial reflection of the primary beam, the penetration of the absorbed primary beam, and the creation and emergence of the secondaries. For example, enhanced surface ionization could occur due to scattering of the primary beam along the surface. This suggestion was based on observations of "resonance effects" in Auger emission (enhancement of the emission from the surface for certain energies of the incident beam).

Acknowledgments.

The authors thank D. Roptin and J. Pillon for their contribution to the material included in this paper. They wish to thank very sincerely Dr Jorgen Schou for his very attentive and very scrupulous reading of their paper as well as for his numerous and stimulating suggestions.

References

Aebi P, Erbudak M, Leonardi A and Vanini F (1987). Electronic excitations and their relaxations in clean and oxidized zirconium surfaces measured in EELS, J. Electron Spectrosc. Relat. Phenom. 42, 351-358.

Argile C, Barthes-Labrousse MG and Rhead GE (1984). Secondary electron emission changes due to metal monolayer adsorption, Surf.Sci.**138**, 181-191.

Austin L and Starke H (1902). Uber die Reflexion der Kathodenstrahlen und eine damit verbundene neue Erscheinung sekündarer Emission, Ann Phys. **9**, 271-292.

Baroody EM (1950). A theory of secondary electron emission from metals, Phys. Rev. **78**, 780-786.

Bindi R, Lanteri H and Rostaing P (1980). A new approach and resolution method of the Boltzmann equation applied to secondary electron emission by reflection for polycristalline Al. J. Phys. D - Appl. Phys.**13**, 267-280.

Bindi R, Lanteri H and Rostaing P (1987). Secondary electron emission induced by electron bombardment of polycristalline metallic targets. Scanning Microscopy, **1**, 1475-1490.

Braundmeier AJ Jr. Williams MW. Arakawa ET and Ritchie RH (1972). Radiative decay of surface plasmons from Al, Phys. Rev. **B5**, 2754-2763.

Bronshtein IM and Segal RB (1960a). Inelastic scattering of electrons and secondary electron emission in certain metals. I, Sov. Phys. Solid state, **1**, 1365-1374.

Bronshtein IM and Segal RB (1960b). Inelastic scattering of electrons and secondary electron emission in certain metals. II, Sov. Phys. Solid state, **1**, 1375-1382.

Bronshtein IM and Fraiman BS (1961). Inelastic scattering of electrons and secondary electron emission from certain metals and semiconductors, Sov. Phys. Solid state, **3**, 1188-1196.

Bronshtein IM and Denisov SS (1965). Effect of the work function on parameters of secondary electron emission, Sov. Phys. Solid state, **6**, 1515-1518.

Bronshtein IM, Stozharov VM and Pronin VP (1972). Angular and energy distribution of electrons inelastically reflected from solids, Sov. Phys. Solid state, **13**, 2821-2826.

Bruining H (1954). Physics and application of secondary electron emission (Pergamon, London).

Cailler M (1969). Contribution à l'étude théorique de l'émission électronique secondaire induite par bombardement électronique, Thèse d'Etat, Université de Nantes.

Cailler M and Ganachaud JP (1972). Quelques aspects théoriques de l'émission électronique secondaire du cuivre, produite par bombardement d'électrons de faible énergie, J.Physique, **33**, 903-913.

Cailler M, Pillon J, Roptin D, Ganachaud JP, Mignot H and Dejardin-Horgues C (1977). Contribution expérimentale et théorique à l'étude de l'émission électronique secondaire. Rapport ATP CNRS (contrat n° 1996) (copy available from M. Cailler).

Chiarello G, Caputi LS, Plutino S, Paolucci G, Colavita E, Decrescenzi M and Papagno L (1984). Aluminum collective excitations : Reflection electron energy loss results, Surf. Sci. **146**, 241-255.

Christensen NE (1976). High-energy band structure of gold, Phys. Rev. **13**, 2698-2701.

Christensen NE and Willis RF (1978). Transmission induced structure in electron emission spectra, Solid State Commun. **25**, 721-724.

Christensen NE and Willis RF (1979). Secondary electron emission from tungsten. Observation of the electronic structure of the semi-infinite crystal, J. Phys. C : Solid State Phys. **12**, 167-207.

Chung MS and Everhart TE (1977), Role of plasmon decay in secondary electron emission in the nearly-free-electron metals. Application to aluminum. Phys.Rev. **15**, 4699-4715.

Cooper BR, Kreiger EL and Segall B (1971). Determination of electron energy bands by phase-shift parametrization : Application to silver, Phys. Rev. **B 4**, 1734-1748.

Copeland PL (1933a). The variation of secondary emission with heat treatment, J. Franklin Institute, **215**, 435-443.

Copeland PL (1933b). Secondary emission of electrons from molybdenum, J. Franklin Institute, **215**, 593-598.

Copeland PL (1935). Secondary emission of electrons from complex targets, Phys. Rev. **48**, 96-98.

Copeland PL (1940). Secondary emission from films of platinum on aluminum, Phys. Rev. **58**, 604-607.

Cornaz A, Erbudak M, Aebi P, Stucki F and Vanini F (1987). Electronic excitations in the transition metals V, Zr, Nb, Mo, and Ta. Phys.Rev. **B35**, 3062-3068.

Devooght J, Dubus A and Dehaes JC (1987). Improved age-diffusion model for low-energy electron transport in solids. I. Theory, Phys. Rev. **36**, 5093-5109.

Dietz RE, McRae EG, Yafet Y and Caldwell CW (1974), Line shape of the 3p excitation in the electron energy-loss spectrum of nickel metal, Phys. Rev. Lett. **33**, 1372-1375.

Dubus A, Devooght J and Dehaes JC (1987). Improved age-diffusion model for low-energy electron transport in solids. II. Application to secondary emission from aluminum, Phys. Rev. **36**, 5110-5119.

Erbudak M, Vanini F, Sulmoni D and Aebi P (1987). Elementary and many-body excitations on surfaces of metals at the beginning of the 4d-series investigted in EELS, Surf. Sci. **189/190**, 771-778.

Everhart TE, Saeki N, Shimizu R and Koshikawa T (1976). Measurement of structure in the energy distribution of slow secondary electrons from aluminum, J. Appl. Phys. **47**, 2941-2945.

Fano U and Cooper JW (1968). Spectral distribution of atomic oscillator strengths, Rev. Mod. Phys. **40**, 441-507.

Farnsworth HE (1925). Electronic bombardment of metal surfaces, Phys. Rev. **25**, 41-57.

Farnsworth HE (1926). Secondary electrons from iron, Phys. Rev. **27**, 413-422.

Farnsworth HE (1928). Energy distribution of secondary electrons from copper, iron, nickel and silver, Phys. Rev. **31**, 405-413.

Feder R and Pendry JB (1978). Theory of secondary electron emission, Solid State Com. **26**, 519-521.

Ganachaud JP and Cailler M (1973). Traitement unifié de l'émission électronique secondaire du cuivre par une méthode de Monte-Carlo, J. Physique, **34**, 91-98.

Ganachaud JP (1977). Contribution à l'étude théorique de l'émission électronique secondaire des métaux, Thèse d'Etat, Université de Nantes.

Ganachaud JP and Cailler M (1979 a), A Monte-Carlo calculation of the secondary electron emission of normal metals. I. The model, Surf. Sci. **83**, 498-518.

Ganachaud JP and Cailler M (1979 b), A Monte-Carlo calculation of the secondary electron emission of normal metals. II. Results for aluminium, Surf. Sci. **83**, 519-530.

Goto K. and Ishikawa K (1972). Method for detecting fine structure in the secondary electron emission yield and the application to Si (111), J. Appl. Phys. **43**, 1559-1562.

Hachenberg O and Brauer W (1959). Secondary electron emission from solids, Adv. Electron. Electron. Phys. **11**, 413-499.

Harrower GA (1956). Auger electron emission in the energy spectra of secondary electrons from Mo and W. Phys. Rev. **102**, 340-347.

Henrich VE (1973). Role of bulk and surface plasmons in the emission of slow secondary electrons. Polycrystalline Aluminum, Phys. Rev. **B7**, 3512-3519.

Hermanson J, Anderson J and Lapeyre G (1975). Observations of f-band final-state structures in gold by ultra-violet photoemission spectroscopy, Phys. Rev. **B12**, 5410-5414.

Hornemann D and Jahrreiss H (1976). Winkelverteilungsmessungen an sekundärelektronen von dünnen metallaufdampfschichten, Vakuum tecknik, **25**, 99-103.

Jahrreiss H and Oppel W(1972). Angular distribution of secondary electrons originating from thin films of different metals in reemission and transmission, J. Vac. Sci. Technol. **9**, 173-176.

Koshikawa T, Shimizu R, Goto K and Ishikawa K (1973). Secondary electron emission from a Fe (110) single crystal, J. Appl. Phys. **44**, 1900-1901.

Koshikawa T, Shimizu R, Goto K and Ishikawa K (1974). Secondary electron energy spectra of single crystal Fe (110) at various emission angles, J. Phys. D : Appl. Phys. **7**, 462-471.

Lang B (1977). Secondary electron spectroscopy of platinum and carbon surfaces, Surf. Sci. **66**, 527-541.

Lanteri H, Bindi R and Rostaing P (1988). Transport models for backscattering and transmission of low-energy (< 3 kilovolts) electrons from solids. Scanning Microscopy, **2**, 1927-1945.

Nozieres P and Pines D. (1958). A dielectric formulation of the many-body problem : Application to the free-electron gas, Il Nuovo cimento, **IX**, 470-490.

Nozieres P and Pines D. (1959). Electron interaction in solids. Characteristic energy loss spectrum, Phys. Rev. **113**, 1254-1267.

Nygaard KJ (1975). Electron impact autoionization in heavy alkali metals, Phys. Rev. **A11**, 1475-1478.

Oppel W and Jahrreiss H (1972). Messungen der winkelverteilung von sekundärelektronen an dünnen freitragenden Al- und Au-schichten, Z. Physik, **252**, 107-117.

Palacio C, Sanz JM and Martinez-Duart JM (1987). Low energy electron emission and EELS of clean and oxidized zirconium, Surf. Sci. **191**, 385-394.

Pattinson EB and Harris PR (1972). Secondary electron spectroscopy of polycrystalline silver, J. Phys. D : Appl. Phys. **5**, L59-L 65.

Pillon J, Roptin D and Cailler M (1976). Secondary electron emission from aluminium, Surf.Sci. **59**, 741-748.

Pillon J, Ganachaud JP, Roptin D, Mignot H, Dejardin-Horgues C and Cailler M (1977). Secondary electron emission of metal surfaces (Al, Ag,Au), Proc. 7th Intern. Vac. Congr. & 3rd Intern. Conf. solid surfaces (Vienna), F. Berger & Söhne, Horn, 473-476.

Pines D (1953). A collective description of electron interactions : IV. Electron interaction in metals. Phys. Rev. **92**, 626-636.

Pines D (1956). Collective energy losses in solids. Rev. Modern Phys. **28**, 184-194.

Pines D (1960). Plasma oscillations of electron gases, Physica, **26**, S 103-123.

Puff H (1964). Zur theorie der sekundärelektronenemission. Der transportprozess, Phys. Stat.

Sol. **4**, 125-365.

Raether H (1965). Solid state excitations by electrons, in Springer tracts in modern physics, ed. Höhler G. (Springer, New york) **38**, 84-156.

Ritchie RH (1957). Plasma losses by fast electrons in thin films, Phys. Rev. **106**, 874-881.

Ritchie RH and Eldridge HB (1962). Optical emission from irradiated foils. I. Phys. Rev. **126**, 1935-1947.

Ritchie RH (1963). On surface plasma oscillations in metal foils, Prog. Theor. Phys. (Kyoto), **29**, 607-609.

Ritchie RH. and Ashley JC (1965). The interaction of hot electrons with a free electron gas, J. Phys. Chem. Solids, **26**, 1689-1694.

Ritchie RH and Marusak AL (1966). The surface plasmon dispersion relation for an electron gas, Surf. Sci. **4**, 234-240.

Ritchie RH (1968). Radiative decay of tangential surface plasmons, Phys. Lett. **27A**, 660-662.

Ritchie RH (1972). Surface plasmons and the image force in metals, Phys. Lett. **38a**, 189-190.

Ritchie RH (1973). Surface plasmons in solids, Surf. Sci. **34**, 1-19.

Ritchie RH, Ferrell TL and Ashley JC (1990). Plasmons in electron spectra, Scanning Microscopy, Supplement 4, 45-56.

Roptin D (1975). Etude expérimentale de l'émission électronique secondaire de l'aluminium et de l'argent. Thèse de Docteur-Ingénieur, ENSM et Université de Nantes.

Rösler M and Brauer W (1981a). Theory of secondary electron emission. I. General theory for nearly-free-electron metals, Phys. Stat. Sol. (b) **104**, 161-175.

Rösler M and Brauer W (1981b). Theory of secondary electron emission. II. Application to aluminum, Phys. Stat. Sol. (b) **104**, 161-175.

Rösler M and Brauer W (1988). Theory of electron emission from solids by proton and electron bombardment, Phys. Stat. Sol. (b) **148**, 213-226.

Rudberg E (1936). Inelastic scattering of electrons from solids, Phys. Rev., **50**, 138-150.

Schäfer J. Schoppe R. Hölzl J. and Feder R (1981). Surf. Sci. **107**, 290-304.

Scheibner EJ and Tharp LN (1967). Inelastic scattering of low energy electrons from surfaces, Surf. Sci., **8**, 247-265.

Schou J (1980). Transport theory for kinetic emission of secondary electrons from solids, Phys. Rev., **B22**, 2141-2174.

Schou J (1988). Secondary electron emission from solids by electron and proton bombardment, Scanning Microscopy, **2**, 607-632.

Seiler H (1983). Secondary electron emission in the scanning electron microscope, J. Appl. Phys. **54**, R1-R18.

Seiler H (1984). Secondary electron emission, Proceedings of the First Pfefferkorn Conference on Electron beam interaction with solids, (SEM Inc., AMF O'Hare,Il.) 33-42.

Sickafus EN (1977a). Linearized secondary-electron cascades from the surfaces of metals. I. Clean surfaces of homogeneous specimens, Phys. Rev. **B16**, 1436-1447.

Sickafus EN (1977b). Linearized secondary-electron cascades from the surfaces of metals. II. Surface and subsurface sources, Phys. Rev. **B16**, 1448-1458.

Smith NV (1974). Photoemission spectra and band structures of d-band metals. III. Model band calculations on Rh, Pd, Ag, Ir, Pt, and Au, Phys.Rev. **B9**, 1365-1376.

Stolz H. (1959) Zur theorie der Sekundärelektronenemission von Metallen. Der transportprocess, Ann. Phys. **3**, 197-210.

Streitwolf HW (1959). Zur theorie der sekundärelektronenemission von metallen der anregungsprozess, Ann. Phys. **3**, 183-196.

Thomas RE, Shih A and Haas G.A (1978). Electron energy loss and secondary emission mechanisms in BaO, Surf.Sci. **75**, 239-255.

Willis RF and Christensen NE (1978). Secondary-electron emission spectroscopy of tungsten : Angular dependence and phenomenology, Phys. Rev. **B18**, 5140-5161.

Willis RF and Feuerbacher B (1975). Angular-resolved secondary-electron-emission spectroscopy of clean and adsorbate covered tungsten single -crystal surfaces, Surf. Sci. **53**, 144-155.

Willis RF, Feuerbacher B and Fitton B (1971a). Graphite conduction band states from secondary electron emission spectra, Phys. Letters, **34A**, 231-233.

Willis RF, Feuerbacher B and Fitton B (1971b). Experimental investigation of the band structure of graphite. Phys. Rev. **B4**, 2441-2452.

Willis RF, Fitton B and Painter GS (1974) Secondary-electron emission spectroscopy and the observation of high-energy excited states in graphite: Theory and experiment, Phys. Rev. **B9**,1926-1937.

Willis RF, Feuerbacher B and Fitton B (1976). Adsorbate-induced surface resonances on tungsten at energies above the vacuum level, Solid State Commun. **18**, 185-189.

Willis RF, Feuerbacher B and Christensen NE (1977). Surface resonance bands on (001) W : Experimental dispersion relations, Phys. Rev. Lett. **38**, 1087-1091.

Wolff PA (1954). Theory of secondary electron cascade in metals, Phys. Rev., **95**, 56-66.

Zimmer HG, Westphal D, Kleinherbers KK and Goldman A (1984). On the analysis of secondary electron emission spectra, Surf. Sci. **146**, 425-437.

Discussion with Reviewers

J. Schou : From your calculations as well as the experiments by Jahrreiss and Oppel (1972) and Oppel and Jahrreiss (1972) one notes that the angular distribution of the emitted (true) secondaries is a cosine distribution. This is striking compared with neutral particle emission, i.e. sputtering, for which the cosine distribution is the exception rather than the rule (Lam, these proceedings). I suppose that you agree in the statement that the cosine distribution for the electrons is a consequence of the isotropic internal distribution of electrons (Hachenberg and Brauer (1959), Rösler and Brauer (1981), Schou (1980) and Ganachaud and Cailler (1979b). Do your simulations show any significant deviations from the cosine distribution (or the internal isotropic distribution) at low energies, e.g. below primary energies of 100 eV? Are there any deviations for the secondaries that are generated directly by the backscattered electrons ?

Authors : In Al, our calculations indicate that the true secondary electrons have a nearly cosine distribution even for energies as low as 100 eV (Ganachaud and Cailler (1979b). These theoretical results are in good agreement with the experimentally observed distributions which, unfortunately, are the most often measured at high primary electron energies. For the backscattered electrons, the angular distribution depends strongly on the primary energy so that for an energy less than 100 eV, the eccentricity parameter χ introduced by Jahrreiss and Oppel can reach values as high as 2. Again, a quantitative comparison with experimental results is unfortunately not directly possible in the absence of measurements in this energy domain. However, according to Jahrreiss and Oppel the variation of χ with respect to the primary energy should be somewhat universal and it was shown by Hornemann and Jahrreiss (Vakuum Technik,25,(1976) p.99) that there is a maximum in the eccentricity *vs.* primary energy curve. A similar observation was performed by Ganachaud (1977) in a theoretical simulation of the secondary electron emission from gold.

The origin of the cosine distribution for the true secondary electrons has never been completely determined, however valuable work on this topic can be found in Ganachaud's thesis (1977) or in papers quoted in the question. From this work it can be thought that the external cosine distribution is the result of an internal isotropic distribution near the surface and of the surface transmission effect. A description of the escape function for the $L_{23}VV$ Auger electrons was also given by Cailler and co-workers (see for instance, Cailler, Barzine and Ganachaud, Surface Sci. 154 (1985), p.548). Whatever the interest of these different studies is, a more complete description of the secondary electron escape function has to be undertaken. A very complete description should take into account the directional effects inside the target as well as the transmission function dependence on the surface roughness and the quantum mechanical effects.

J. Schou : Could you explain why the spectrum for Al_2O_3 is much narrower than for pure aluminium?

Authors : The width of the secondary peak is a very used parameter for the characterization of the secondary electron peak but in no way, the only important characteristic. In fact, a secondary electron peak should be described in true amplitude and not only with a maximum height normalized to a unit value. If so, it could be verified in some cases that differences in the shape of the secondary electron peak could result principally from a decrease in the height of the peak and from a shift in the location of the zero of energy. An example of this was obtained on gold samples (CaillerM, Pillon J, Roptin D, Ganachaud JP, Mignot H and Dejardin-Horgues C. "Contribution expérimentale et théorique à l'étude de l'émission électronique secondaire, Contrat ATP CNRS n°1996, 1977). For Al samples it was experimentally found that the height of the secondary electron peak for the oxidized target was much larger than for sputtered specimen and that there was a shift in the location of the zero of energy. This should be connected with the fact that the Al_2O_3 layer is a rather thick insulator layer. Unfortunately, no experimental proof of the differences in amplitude can be shown at the present time. A second explanation is to be looked for in the contributions to the secondary electron emission of the bulk and the surface plasmon damping. Indeed, for sputtered Al, the plasmon damping mechanisms bring a very important contribution to the secondary electron emission (very roughly 50%) and because of the plasmon energies, they determine for the essential, the width of the true secondary peak. The shoulders in the shape of the secondary electron peak can appear rather weak

but in fact, they are only "the emerged part of the iceberg". The secondary electron emission from the oxidized target is higher than that from the sputtered specimen but apparently does not exhibit plasmon damping contributions.

J. Schou : What is the main reason for the fast decrease of the electron spectra at the high energy side (Figs. 3 and 5-7)? Do the authors agree in the statement that decrease is primarily caused by the strongly increasing stopping power for the low-energy electrons (comp. Schou (1980)), or in analogy with this, a strongly reduced mean-free-path for the emerging electrons in the solid with increasing energy (compare Fig.2 in Ganachaud and Cailler (1979a))?

Authors : This is probably the good answer.

R. Bindi : Could you say something about the suitable orientations in experimental observations and theoretical description of secondary electron emission?

Authors : Different complementary orientations seem to be interesting. The first one is connected with an extension of theoretical models to materials other than Al in order to simulate the final-state effects. From this point of view, the introduction of autoionization emission has to be performed. A second orientation is the study of insulators. A third one is the study of surface effects (transmission function, source function, etc.) on the secondary electron emission properties. Finally, a study of the secondary electron emission of materials covered with a thin film could bring informations on the absolute values of the mean free paths. It should also be interesting to study the effects of the interface roughness and, for instance, to explore if there is a relation between the secondary electron emission properties of the samples and the adhesion strength of the coating on its substrate.

M. Kotera : Can you evaluate the influence of the autoionization process including Auger effect on the total amount of secondary generation in the specimen?

Authors : At time, no theoretical study of the autoionization emission contribution to secondary electron emission was performed. As mentionned above, it should be an interesting orientation for future works.

P. Nordlander : How different is the secondary emission induced under similar energy bombardment using ions, electrons or X-rays?

Authors : Concerning the transport of the electrons which have been excited in the solid by electrons, by ions or by X-rays, the situations are very similar. On the contrary, some striking differences can occur in the excitation processes. A very interesting review paper on the comparison between the secondary electron emission from solids induced by electron and ion bombardment was written by Schou (1980), in which the interested reader will find many detailed informations. As indicated by Schou, the basic interaction between a primary electron or a proton and the target electrons are similar. However, there are some differences, for instance, when a light particle like an electron interacts elastically with an ion in the solid, it can experience large backscattering effects. This is not the case when the incident particle is an ion, so that, for instance, there is no backscattered proton beam at sufficiently high energies of the primary beam. Therefore, in that case, and contrarily to the secondary electron emission induced by electron bombardment, all the secondary electrons are created by the penetrating proton beam. In spite of these differences and as reported by Schou, the energy distribution of the emitted secondaries obtained in both cases are fairly similar.

The situation is complex for heavier ions because of the possibility of modification in the target (knock-on effects for instance) or in the primary ion charge state.